Engineering nanotechnological applications of biomolecular motors and microtubules

DISSERTATION

submitted for the degree of

Doctor of Philosophy

(PhD)

at the

Department of Chemistry

Fakultät für Mathematik und Naturwissenschaften

Technische Universität Dresden

by

Samata Chaudhuri

born on March 21st, 1990 in Kolkata, India

October, 2017

Reviewers:

1. Prof. Dr. Brigitte Voit
   Department of Chemistry and Food Chemistry, TU Dresden
   Leibniz Institute of Polymer Research Dresden (IPF)
   Hohe Str.6, 01069 Dresden.

2. Prof. Dr. Stefan Diez
   B CUBE - Center for Molecular Bioengineering, TU Dresden
   Arnold Str.18, 01307 Dresden.

The work described in this thesis was conducted at the Max Planck Institute of Molecular Cell Biology and Genetics, and the B CUBE – Center for Molecular Bioengineering, both located in Dresden, Germany.

In the loving memory of my grandmother, Mrs. Bani Mitra.

Abstract

Biomolecular motor based transport reconstituted in synthetic environment has been recently established as a promising component for the development of nanoscale devices. A minimal system consisting of microtubules propelled over a surface of immobilized kinesin motor proteins has been used to transport and manipulate cargo for molecular sorting, analyte detection, and other novel nanotechnological applications. Despite these achievements, further progress of the field and translation of the reported applications to a real-world setting require overcoming several key challenges, such as, development of effective cargo conjugation strategies and precise control of the transport directionality with the reconstituted biomolecular motor systems.

The challenge of cargo conjugation is addressed in this thesis through the development of a robust bioorthogonal strategy to functionalize microtubules. The versatility of the developed method is demonstrated by covalently conjugating various types of cargos to microtubules. Further, the effect of the linker length on cargo attachment to microtubules is investigated by attaching cargo to microtubules *via* linkers of different lengths. By using kinesin-driven transport of microtubules that are covalently conjugated to antibodies, detection of various clinically relevant analytes is demonstrated as proof-of-principle applications for biosensing. Finally, the challenge of gaining control over transport directionality is addressed through topographical guiding of microtubules in nanostructures, and optimization of assay parameters to achieve successful guiding of microtubules. Spatio-temporal analyte concentration, using transport in these nanostructues, is also explored to make the biomolecular-motor based applications more suitable for use real-world point-of-care setting.

Taken together, the experimental work in this thesis contributes to the field of nanotechnological applications of biomolecular motors. The developed microtubule functionalization method and understanding of the effect of cargo attachment *via* linkers provide useful design principles for efficient cargo loading to microtubules. Moreover, establishment of assay components for successful guiding of microtubules in nanostructures is a vital step forward for practical translation of future nanoscale devices.

Contents

List of Figures

LIST OF FIGURES

Glossary

E.coli	*Escherichia coli*
Ab-MT	Antibody-conjugated microtubules
Abl	Abelson murine leukemia viral oncogene
ADP	Adenosine-5'-diphosphate
ATP	Adenosine-5'-triphosphate
Bcr	Breakpoint cluster region
CuAAC	Copper(I) catalyzed azide alkyne cycloaddition
DMSO	Dimethyl sulfoxide
DTT	Dithiotreitol
EDTA	Ethylene-diamine-tetraacetic acid
EGTA	Ethylene-glycol-tetraacetic acid
ELISA	Enzyme-linked immunosorbent assay
EMCCD	Electron multiplying charge-coupled device
F.I.	Fluorescence intensity
FIESTA	Fluorescence Image Evaluation Software for Tracking and Analysis
GDP	Guanosine-5'-diphosphate

GLOSSARY

GMPCPP Guanosine 5'-[α,β-methylene] triphosphate

GTP Guanosine-5'-triphosphate

iEDDA Inverse electron demand Diels Alder addition

IgG Immunoglobulin G

MAPs Microtubule associated proteins

MW Molecular weight

NHS N-hydroxysuccinimide

PBS Phosphate buffer saline

PDMS Poly(dimethylsiloxane)

PEG Poly(ethyleneglycol)

PIPES Piperazine-N,N-bis(2-ethanesulfonic acid)

PLL Poly(L-lysine)

rpm Revolutions per minute

SA Streptavidin

SPAAC Strain promoted azide alkyne cycloaddition

TCO *Trans*-cyclooctene

TIRF Total internal reflection fluorescence

Tris 2-Amino-2-hydroxymethyl-propane-1,3-diol hydrogen chloride

1

Introduction

Nature has evolved over billions of years to make life the wonder that it is. Cells, the basic building blocks of life, are capable of carrying out a vast array of complex functions with its elegantly evolved molecular machinery. For example, biomolecular motor proteins, in conjunction with their associated cytoskeletal filaments, constitute the highly-efficient intracellular transport system in the cells. These proteins actively transport cellular cargo, position various cellular components, and are key players in vital physiological functions such as cell division. Taking inspiration from nature, an active area of nanotechnological research has been focused at emulating nature's machinery by reconstituting this highly efficient, cellular transport in synthetic environments to develop novel applications. In recent years, kinesin motor proteins along with microtubule filaments have proved to be promising candidates for the development of such synthetic biohybrid devices[1–11]. In this thesis, the quest to develop nanotechnological applications with biomolecular motors is explored using the motor protein - kinesin-1 and its associated cytoskeletal filament - microtubules.

1.1 The cellular cytoskeleton

The cytoskeleton of the cell is composed of an intricate network of filaments (such as actin and microtubules) which constitutes the tracks over which the motor proteins (such as myosin on actin, and kinesin on microtubules) transport

cargo. In the following sections, an overview of the kinesin motor protein and the microtubule filaments, which are used in this thesis, is presented.

Kinesin

Kinesin was discovered by Vale and colleagues in 1985 as the biomolecular motor responsible for fast transport of organelles along the microtubules in the axons of giant squids[12]. Based on the ability of this protein to induce motility, they named it Kinesin (from the Greek word *kinein*, meaning "to move"). Since then, further studies have led to the discovery of a large number of proteins that are structurally and functionally similar to the first kinesin in various organisms. These proteins, along with the kinesin reported by Vale et al.[12] ("Kinesin-1"), constitute the kinesin superfamily of motor proteins.

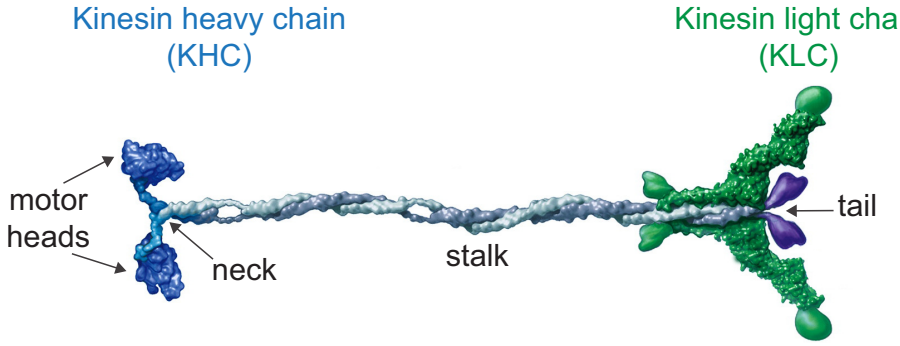

Figure 1.1: The structure of Kinesin-1 - Kinesin-1 is composed of two identical kinesin heavy chains (KHC) and kinesin light chains (KLC). Adapted from Vale, 2003[13]

The kinesins move along the microtubules to transport organelles, vesicles, and other molecules, and also participate in spindle organization and the transport and separation of chromosomes during cell division[14–18]. In this thesis, kinesin-1, the first discovered as well as the best characterized kinesin, has been used and will be further described. Kinesin-1 is a $\sim$ 360 heterotetrameric protein consisting of two heavy chains (kinesin heavy chain or KHC, $\sim$ 120 kDa) and two light chains (kinesin light chain or KLC, $\sim$ 60 kDa)[19–21]. The KHCs in turn consist of N-terminal motor domains called "heads", connected with a "neck linker". This

region is followed by a coiled-coil region called the "stalk" that facilitates the dimerization of the protein[22]. The heavy chain terminates with the C-terminal "tail" region, that connects to the KLCs. The tail is responsible for cargo binding; in the absence of any cargo, the tail domain folds back and binds to the motor heads[23], rendering the motor inactive. The KLCs consist of N-terminal coiled-coil domain, followed by a tetratricopeptide repeat and a C-terminal domain. The domains of the KLC recognize and bind to different regions of the cargo and facilitate cargo-transport by the motor (Figure 1.1).

Kinesin-1 moves to the plus end of a microtubule in a "hand-over-hand" fashion[24,25]. It is a highly processive motor, enabling it to take several steps before detaching from the microtubule. One of the two motor heads is always bound to the microtubule[26], while the other takes a 16 nm step by deriving energy from the hydrolysis of one molecule of ATP to ADP[23,27]. Consequently, the motor covers a distance of 8 nm for each molecule of ATP hydrolyzed. During its movement, a single kinesin-1 molecule can exert a force upto 6 pN[27,28]. This results in an energy production of 48 pN $\cdot$ nm per step of the motor, per molecule of ATP consumed, corresponding to an incredibly high energy efficiency of $\sim$ 50 % for the conversion of chemical energy of ATP to mechanical work.

Microtubules

Structure and dynamics

Microtubules are stiff, hollow cylindrical structures that provide mechanical support to the cells to maintain their shapes. Additionally, they constitute the tracks on which molecular motors, such as kinesin, transport their cargos inside the cell.

Microtubules are polymers composed of α - and β - tubulin heterodimers. The tubulin monomers (MW $\sim$ 55 kDa) share almost 50% homology in their primary sequence[29]. Each of the α and β tubulin monomer binds to a GTP nucleotide. The GTP bound to the α - tubulin is non-hydrolyzable, while that bound to the β - tubulin can be hydrolyzed to GDP. To polymerize microtubules, tubulin heterodimers with GTP bound to both α and β subunits assemble in a head-to-tail manner to form polar protofilaments with α - tubulin exposed at the

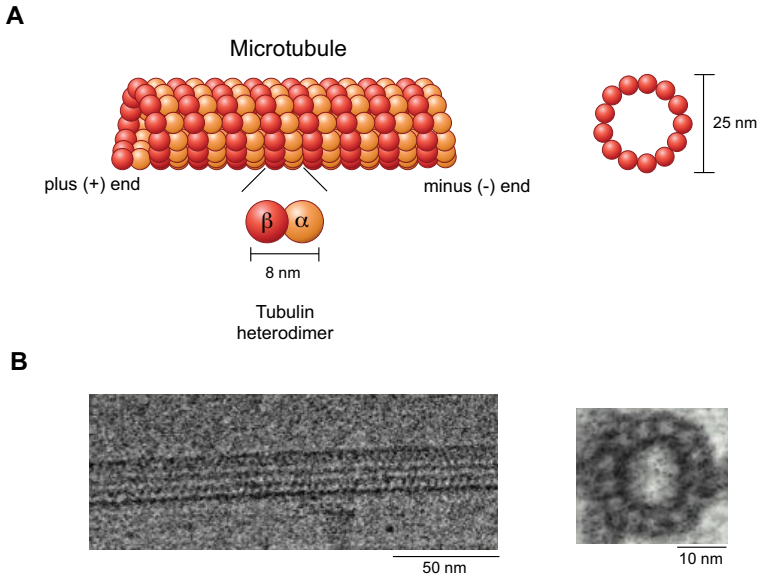

Figure 1.2: The structure of microtubule - (A) Microtubules are assembled from tubulin heterodimers to form stiff hollow tube composed of 13 protofilaments. (B) Electron micrograph of a short segment of microtubule (left image) and the microtubule cross-section (right image). Adapted from Alberts,2004.

minus end and β - tubulin at the plus end. During this polymerization process, the GTP bound to the β-subunit is hydrolysed to GDP, as the β-subunit of the heterodimer binds to the α-subunit of the next heterodimer of the protofilament. The protofilaments bind laterally to form a hollow cylinder with an outer diameter of about 25 nm and inner diameter of about 15 nm[30,31] (Figure 1.2). *In vivo*, microtubules are predominantly composed of 13 - 14 protofilaments, while *in vitro* the number of protofilaments in a microtubule can vary from 10 to 15[26,31,32](179), with most microtubules consisting of 14 protofilaments[31].

Microtubules exhibit the phenomena of dynamic instability, characterized by phases of slow growth and rapid shrinkage[33]. In a polymerizing microtubule, the hydrolysis of the GTP at the plus end is slower than the rate of polymerization (that is, addition of a new tubulin dimer)[34,35]. This results in the formation of a GTP "cap" at the plus end, which stabilizes the growing microtubule. Loss of the GTP cap, destabilizes the microtubule, resulting in depolymerization of the microtubule ("catastrophe"). Reversal to a state of microtubule polymerization is

possible through the attachment of sufficient tubulin dimers with non-hydrolyzed GTP at the plus end ("rescue"). The dynamic instability of microtubules allows cells to regulate microtubule length and distribution for reconfiguration of the cytoskeleton during cell division or development[36].

Chemical stabilization of microtubules *in vitro*

In vitro microtubules can be stabilized by various chemicals to slow down depolymerization. In this thesis, three different methods to grow and stabilize microtubules have been used:

1. Microtubule polymerization with GTP, followed by stabilization with Taxol. Taxol, a commonly used anti-cancer drug, stabilizes microtubules by preventing GTP hydrolysis[37,38].

2. Microtubule polymerization with slowly hydrolysable GTP analogues like guanylyl-(alpha, beta)-methylene-diphosphonate (GMP-CPP). Stabilization with GMP-CPP results in almost 5000 fold decrease in microtubule depolymerization rate[39].

3. Microtubule polymerization with GMP-CPP, followed by stabilization with Taxol.

Polymerized microtubules can also be chemically cross-linked with glutaraldehyde to extend their lifetimes[40].

1.2 Engineering nanotechnological applications

Owing to their small size, energy efficiency, and robustness in synthetic environments kinesins and microtubules are an attractive choice for a wide range of nanotechnological applications[1–11]. To reconstitute the biomolecular transport *in vitro*, two types of assay geometries are commonly used:

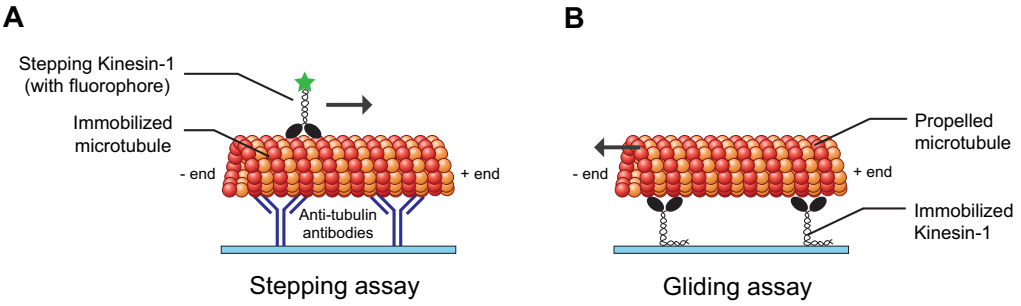

Figure 1.3: *In vitro* reconstitution of biomolecular transport - (A) Stepping assay of fluorescent kinesin molecules walking on microtubules immobilized with anti-tubulin antibodies. (B) Gliding assay of microtubules propelled over a surface of immobilized kinesin-1 motors.

Stepping assay Here, microtubules are immobilized on a surface (*via* anti-tubulin antibodies or other means) and the kinesin motors move over them (Figure 1.3A). This assay geometry has been used to transport cargos such as beads[41], nanosphere[40], oil droplets[42] along the surface immobilized microtubules. The distance through which the cargo gets transported depends on the length of the microtubule over which the cargo-transported kinesins are moving, unless the immobilized microtubules are overlapping.

Gliding assay Also called "inverted motility assay", the microtubules are transported in this case over a surface of immobilized kinesin motors[43](Figure 1.3B). As the microtubules are propelled by the collective action of multiple motors, this assay results in more robust cargo transport *via* cargo conjugated microtubules. Consequently, this geometry is a popular choice for biomolecular motor-based nanotechnological applications, and is used in this thesis.

Engineering challenges

Reconstitution of biomolecular motor and microtubule motility *in vitro* has resulted in the development of a wide range of nanotechnological applications. This energy-efficient, nanoscale system has been used as molecular transporter for cargo loading and unloading[7,11], molecular sorting[9], surface imaging[44], and

biosensing[6,45]. However, there have been two major challenges to the development of these biomolecular-motor-based applications: 1. Development of successful cargo conjugation methods, 2. Achieving control of the microtubule transport

Cargo conjugation strategies Attachment of cargo to microtubules is crucial for the development of a vast majority of biomolecular motor-based nanotechnological applications. Ideally, the bioconjugation strategy used to conjugate cargo to microtubules should be facile, specific, efficient, and applicable for the attachment of a wide range of cargo, without compromising the activity of the biomolecules involved (kinesin, microtubule, etc.).

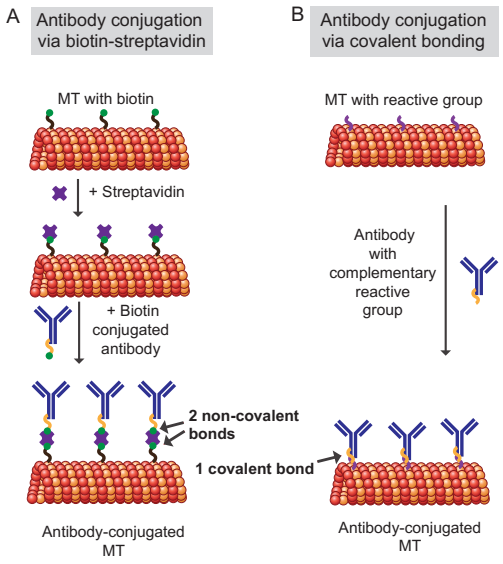

Figure 1.4: Comparison of schemes to conjugate cargo (here, antibodies) to microtubules using A. biotin-streptavidin (left) and B. covalent conjugation (right). - In case of A, antibodies are attached to the microtubule *via* two non-covalent bonds between biotin-streptavidin, each with its characteristic dissociation constant. On the other hand, for B, the antibodies are attached to the microtubule *via* single covalent bond, yielding a stable conjugate.

Over the years, cargo conjugation to microtubules has been achieved by employing both non-covalent and covalent strategies. Until now, the non-covalent interaction between biotin and streptavidin has been the most popular choice for cargo conjugation[1,2,4,5,7–11]. Despite being the strongest non-covalent bond known, with dissociation constant (K_d) of $10^{15} M$[46,47], the biotin-streptavidin linkage is limited by non-specific clustering and aggregation[48,49], and decreased lifetime of the bond under tension[50–52]. Cargo loading to microtubules has also been achieved using DNA hybridization[11,53–56]. As the

DNA strands were conjugated to the cargo and/or microtubules *via* biotin-streptavidin linkage, these applications were limited by the drawbacks intrinsic to the biotin-streptavidin bond. Covalent approaches were used to modify microtubules by chemically cross-linking microtubules with glutaraldehyde[6], functionalizing microtubules with succinimidyl-4-hydrazidoterephthalate (SHTH)[57] or N-hydroxysuccinimidyl (NHS)-ester agents. These chemicals modify the primary amino acids of any protein, and are therefore non-specific in nature. Site-specific cargo conjugation to microtubules was achieved by expression and purification of non-natural amino acid incorporated recombinant tubulin, followed by selective modification of these residues to allow bioorthogonal "click" reaction for cargo attachment[58]. However, successful expression of recombinant tubulin is limited by low yield and tubulin aggregation[59], which in turn limits the practical applicability of any recombinant-tubulin based cargo loading strategy. Früh et al.[60] applied bioorthogonal "click chemistry" to successfully conjugate fluorescent dye to microtubules in a gliding motility assay. Their reaction was based on the strain-promoted alkyne-azide cycloadditions (SPAAC) reaction between azide and strained alkyne. Bioorthognal reactions provide exquisite selectivity in chemically modifying biomolecules without interference or side-reaction with the functionalities present in the biological system (thus are orthogonal to intrinsic biological reactions). Despite the selectivity, SPAAC reactions are limited by their slow kinetics ($k < 1$ /M/s compared to $k_{on} \sim 10^5 - 10^6 M^{-1}s^{-1}$ for affinity-ligand-based reactions)[61,62]. For practical applications of bioorthogonal reactions, kinetic rates of $k \sim 10^3 M^{-1}s^{-1}$ and higher are deemed critical[63]. In this thesis, inverse electron demand Diels-Alder (iEDDA) bioorthogonal reaction between tetrazine and *trans*-cyclooctene - the fastest currently known bioorthogonal reaction - will be employed to covalently conjugate various types of cargo to microtubules.

Control of transport directionality Unlike the highly-specific directional motor transport *in vivo*, reconstituition of biomolecular motor-based transport *in vitro* lacks directionality. Precise control of the direction of transport is critical for further exploitation of the advantages of biomolecular system *in vitro* and to translate the reported proof-of-principle applications to a practical setting.

Over the years, various approaches were undertaken by different groups to achieve control over microtubule motility for nanoscale transport. Initial attempts focused on depositing kinesin coated poly(tetrafluoroethylene) (PTFE) films[64], or using microtubules templates to "print" kinesin onto a glass surface[65] that restricted the motion of the microtubules along the films' orientation axes or the printed kinesins respectively. While linear control of microtubules motion was achieved with these methods, unidirectional transport could not be attained. Later, Clemmens et al.[66] used chemical patterning to create alternating kinesin-coated and kinesin-free tracks, and quantified how well the microtubule gliding was confined within the kinesin coated tracks. They observed that the angle at which a microtubule moving in the kinesin-coated track approached the boundary between kinesin-coated and non-coated surface decided the probability of the microtubule to be guided in the desired track. The higher the approach angle, lower is the probability of the microtubule to follow the track and be guided by the chemical patterning. Several groups demonstrated control of microtubule movement by steering the intrinsically negatively charged microtubules with electric field[67–69], or by using magnetic fields to steer $CoFe_2O_4$ functionalized tip of the microtubule[8]. Shear flow has also been used to orient the microtubules in a flow channel and impart directionality to their movement[70,71]. Another strategy involved fabrication of microlithographic tracks and physically restricting the movement of microtubule within them. Microtubules were successfully guided in topographical structures comprising open channels of few micrometers delineated by boundary walls several hundred nanometers high[3,9,66,72–77]. Unidirectional motion of gliding microtubules was achieved by using "rectifier" geometries to guide the microtubules approaching the boundary wall[3,72,74]. Introduction of overhangs on the boundary wall further prevented the loss of approaching microtubules, improving the guiding efficiency of the structures[78]. In this thesis, lithographically patterned channels, modified with selective surface chemistry, will be used to impart directionality to microtubule movement.

1.3 Motivation

The field of nanotechnological applications of biomolecular motors is a young and evolving area of research. While the field has advanced significantly in the recent decades, it is fraught with several engineering challenges (see 1.2). The overarching goal of this thesis is to address some of these current challenges and following that, demonstrate proof-of-principle applications of microtubules and kinesin-1 motors aimed particularly at analyte detection applications.

Of these, the establishment of robust bioconjugation strategies to modify microtubules can provide the much-needed impetus to drive the development of novel applications with microtubules and kinesin motors, particularly for cargo-transport based applications. This is the first engineering challenge that is addressed in this thesis, through the development of a bioorthogonal strategy to functionalize microtubules that overcomes the limitations of the non-covalent cargo conjugation schemes currently used in the field. The developed bioconjugation scheme is then utilized to successfully demonstrate several analyte detection applications.

The second engineering challenge addressed in this thesis is aimed at controlling the directionality of reconstituted microtubule motility to generate useful transport. Fundamental parameters of the reconstituted assay are probed to determine factors that influence successful guiding of microutbules in lithographically patterned nanostructures. Following this optimization, the guided microtubule movement in the nanostructures is employed to achieve spatio-temporal analyte concentration and analyte detection.

1.4 Outline of the thesis

In **chapter 1**, the motor protein - kinesin-1 (referred to as "kinesin" from now on), and its associated cytoskeletal filament - microtubules were introduced, along with the assay setups used to engineer nanotechnologcal applications with these components. The chapter concluded with a review of the current engineering challenges to the development of these applications, along with relevant examples.

The subsequent chapters of the thesis are aimed at addressing these engineering challenges mentioned.

In **chapter 2** of the thesis, a versatile bioorthogonal strategy to covalently conjugate various types of cargo to microtubules is developed. Thereafter, using the developed conjugation strategy, the effect of linker length on cargo attachment to microtubules is investigated. The results from this chapter provides useful design principles to strategize suitable cargo conjugation scheme to microtubules based on the desired application.

In **chapter 3**, microtubules with covalently conjugated antibodies (using the method developed in chapter 2) are used in a kinesin gliding motility assay to develop proof-of-principle biosensing applications. Detection of various clinically relevant analytes is reported using fluorescence-based as well as label-free detection methods.

Finally, **chapter 4** of the thesis investigates the fundamental aspects of the gliding motility assay in lithographically patterned nanostructures. As these structures aim to bridge the current gap at translating the proof-of-principle applications to a practical point-of-care setting, a comprehensive understanding of the basic assay features is undertaken in this chapter that provides useful insights to the development of future nanotechnological applications with biomolecular motors.

2

Bioorthogonal cargo conjugation to microtubules

Transport systems based on biomolecular motors are promising components for developing nanoscale devices[79,80] due to their small-size, energy efficiency,[81] and detection sensitivity[45,82]. A critical requirement for vast majority of these applications is the development of effective microtubule functionalization schemes that ensure reliable cargo loading. Ideally, such schemes are simple, robust, and applicable to a wide range of cargo. Traditionally, the most common method of cargo attachment to microtubules has been using the biotin-streptavidin linkage[1,2,4,5,7–11]. Here, a novel bioconjugation strategy is presented to covalently couple cargo to microtubules using the recently developed inverse-electron-demand Diels-Alder addition (iEDDA)[83,84] reaction between tetrazine and *trans*-cyclooctene (TCO) (Figure 2.1). Besides retaining the advantages of "click chemistry" (including high reaction specificity, and biocompatibility), iEDDA reactions proceed at unprecedented speed ($k > 800 M^{-1}s^{-1}$, faster than any other known bioorthogonal reaction) in a wide range of solvents, and do not require catalysts. Moreover, the recent commercial availability of a wide range of tetrazine and TCO reagents has made iEDDA reactions a popular choice for bioconjugation applications.

Conjugation of two types of cargos - monoclonal IgG antibodies and fluorescent streptavidin - using the TCO-tetrazine bioorthogonal reaction is described. These cargo conjugated microtubules are then used in a kinesin gliding motility assay for the development of various nanotechnological applications in the next chapters.

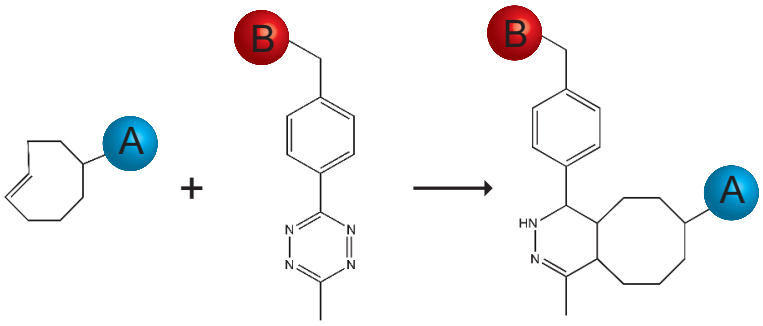

Figure 2.1: Bioconjugation Scheme - Inverse electron demand Diels Alder (iEDDA) reaction between trans-cyclooctene (TCO) functionalized biomolecule A and methyl-tetrazine functionalized biomolecule B.

Previous studies have shown that cargos attached to the microtubules act as obstacles to the kinesin motors that propel the microtubules in a gliding motility assay[85,86]. This phenomenon, called the "roadblock effect", occurs as the cargo hinders the access of the motor heads to their binding site on the microtubules, effectively decreasing the rate at which the motors propel the microtubules forward. The gliding velocity of cargo-conjugated microtubules can go down to as low as 10% of its velocity in the absence of any cargo[85,86]. Despite the scope of applications with biomolecular motors *in vitro*, this compromised transport of microtubules on cargo attachment constitutes a major bottleneck in the field. While a high density of cargo, such as antibodies, on the surface of the microtubules is desirable for various applications, such as biosensing and analyte detection, the corresponding decrease in microtubule velocity with cargo attachments impairs the development of fast detection assay[45]. To overcome these limitations, an alternative strategy to circumvent the "roadblock effect" was explored by attaching cargo to the microtubules *via* long flexible poly-ethylene glycol (PEG) linkers using the developed bioconjugation method.

Publication Results from this chapter (section 2.1) and the next chapter (section 3.1) have been published as: *Tetrazine-trans-cyclooctene-mediated conjugation of antibodies to microtubules facilitates sub-picomolar protein detection.* S. Chaudhuri, T. Korten, and S. Diez. Bioconjugate Chemistry, 28 (4), 918–922 (2017).

2.1 *trans*-cyclooctene functionalization of microtubules

To obtain TCO-functionalized microtubules, tubulin was labeled with TCO-$(PEG)_x$-NHS (where x = 0, 4, 12) by modifying the solvent accessible amino groups of the protein (Figure 2.2A. For details see Section 6.3). Taxol-stabilized microtubules were polymerized from a 4:3:1 mixture of TCO-$(PEG)_x$-tubulin, unlabeled-tubulin, and rhodamine-tubulin, and used in a kinesin gliding assay.

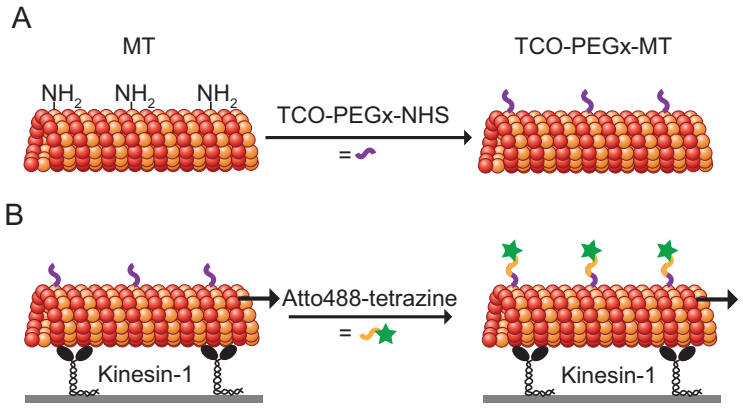

Figure 2.2: Functionalization of microtubules with *trans*-cyclooctene (TCO) - (A) Functionalization scheme. Solvent accessible amino groups of tubulin were modified by TCO-$(PEG)_x$-NHS (x = 0, 4, 12). (B) Scheme for confirmation of TCO-functionalization of microtubules in a kinesin gliding motility assay. To confirm successful labeling, microtubules were polymerized from a 4:3:1 mixture of TCO-$(PEG)_x$-tubulin, unlabeled-tubulin, and rhodamine-tubulin, and used in gliding motility assay where 1 µM Atto488-tetrazine dye was added to confirm the presence of the TCO groups on the microtubules.

For developing gliding-assay-based applications with functionalized microtubules, two important criteria need to be fulfilled: (i) the chemically-modified tubulin should retain its ability to polymerize into microtubules and (ii) the polymerized microtubules in turn should retain their ability to glide over the kinesin surface. To confirm the successful labeling and the accessibility of the TCO-groups on these microtubules, 1 µM fluorescent Atto488-tetrazine dye was added in the gliding motility assay (Figure 2.2B). Following 10 min incubation,

the excess dye was washed off, and the fluorescence intensity of the dye per unit length of the TCO-$(PEG)_x$-microtubules, as well as the gliding velocity of these microtubules, was evaluated. Control microtubules polymerized from Cy5-labeled tubulin were also added to the assay with the TCO-$(PEG)_x$-microtubules. Figure 2.3A shows the plot of microtubule gliding velocity (black data points) and the corresponding signal from Atto488-tetrazine dye (green data points) for different TCO-$(PEG)_x$-microtubules and the control microtubules. The gliding velocities of the TCO-$(PEG)_x$-microtubules were similar to that of the control microtubules, in agreement with previous reports showing that functionalization with small amine-reactive reagents does not significantly affect the gliding motility of microtubules[6,60,87]. However, the signal from the fluorescent tetrazine-dye was found to increase with the increase in number of PEG-units present in the TCO-$(PEG)_x$-microtubules. The fluorescence images of the microtubules (in red) and the signal from the Atto488-tetrazine dye (in green) also showed an increase in signal from the dye for the TCO groups attached *via* longer linkers (Figure 2.3B). Moreover, as the length of the linker increases from 0 PEG units to 12 PEG units, a corresponding increase in the labeling efficiency was observed as quantified from the 4 fold increase in fluorescence signal from the tetrazine dye. These results demonstrate that the presence of a long, flexible PEG linker enhances the labeling efficiency of small-molecule functionalization of tubulin.

Long term storage of PEG-functionalized proteins is often problematic due to the loss of polymeric PEG backbone through oxidation and/or hydrolysis[88]. As the problem is putatively exacerbated by longer length of the PEG chain, the TCO-group with optimal number of PEG linker units was chosen for labeling tubulin. While the presence of longer PEG linker attached to the TCO group was found to improve the labeling, the labeling observed with linker consisting of 4 PEG units was already several fold higher than that without any PEG linker. Therefore, as a 4 unit PEG linker reagent is expected to have better long-term stability over a 12 unit PEG linker reagent, TCO-$(PEG)_4$-NHS labeled tubulin was used for conjugating tetrazine-modified cargo in the following sections.

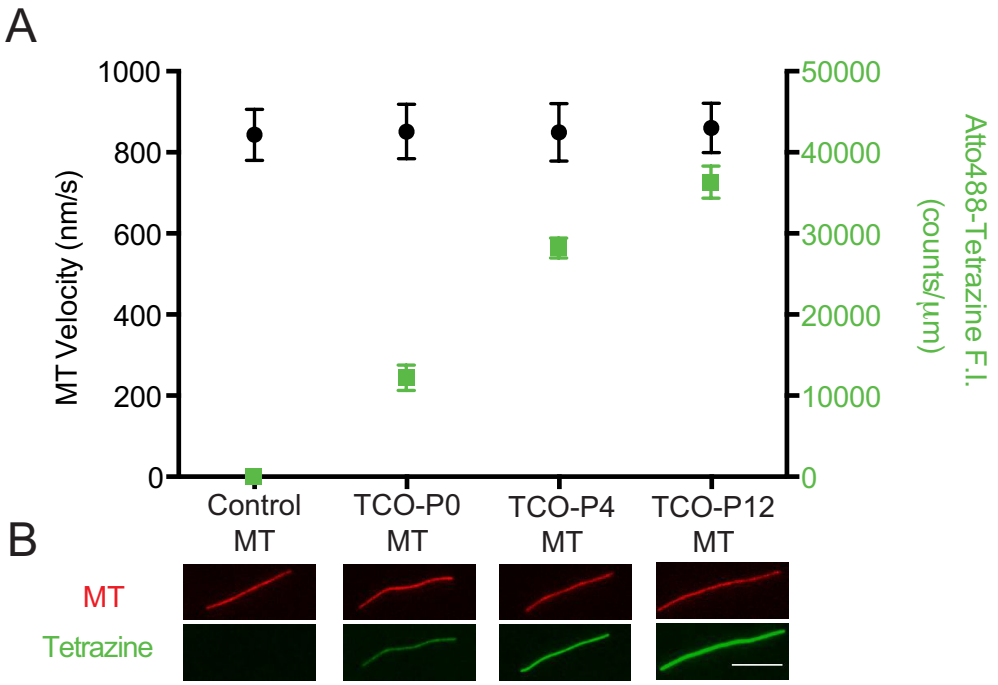

Figure 2.3: Characterization of the TCO-$(PEG)_x$-functionalized microtubules in kinesin gliding motility assay - A. Gliding velocity of the microtubules and the amount of TCO on the microtubule surface. Gliding velocities (black data points) of microtubules polymerized from 4:3:1 mixture of TCO-$(PEG)_x$-tubulin, unlabeled-tubulin, and rhodamine-tubulin showed that the gliding velocity was unaffected by the labeling. The amount of TCO groups on the microtubule surface, as quantified from the fluorescence intensity of the Atto488-tetrazine dye (green data points) per unit length of the microtubule, increased as the number of PEG units *via* which the TCO group was attached increased. Data (mean ± standard deviation) evaluated for 28 – 57 microtubules. B. Fluorescence images of the microtubules (red) and the corresponding signal from the Atto488-tetrazine dye (green). The control microtubules without the TCO group showed no signal in the green channel, while the signal from the TCO-$(PEG)_x$-microtubules increased with the increase in number of PEG units in the linker. Thus, increase in the length of linker for attachment of the TCO group to the microtubules enhances the labeling efficiency. Scale bar 10 μm.

2.2 Attachment of antibodies to microtubules for analyte detection

To generate antibody-conjugated microtubules (Ab-MTs), tetrazine-$(PEG)_5$-modified mouse IgG antibodies were covalently coupled to rhodamine and TCO-$(PEG)_4$-colabeled microtubules (TCO-MTs) using the bioorthogonal iEDDA reaction (Figure 2.4A). To confirm successful conjugation, 100 nM Alexa Fluor 488 anti-mouse secondary antibodies were added to the Ab-MTs surface-immobilized by anti-rhodamine antibodies (Figure 2.4B). Rhodamine-Cy5-colabeled, non-TCO-functionalized microtubules that lacked the tetrazine-modified antibodies were used as control. After 30 min incubation and subsequent washing, specific co-localization of the fluorescent Alexa Fluor 488 signal from the secondary antibodies to the Ab-MTs confirmed successful conjugation (Figure 2.4C). The high intensity and uniform distribution of the co-localized signal indicate a high labeling density of the Ab-MTs. This can be ascribed to the efficiency of the iEDDA reaction, enabling high conjugation of antibodies to the microtubules. Additionally, the presence of short PEG linkers on both the TCO and the tetrazine groups potentially contributes to accentuating the conjugation efficiency by increasing the accessibility to the binding sites.

Next, the Ab-MTs were used in a kinesin gliding motility assay (Figure 2.4D). The Ab-MTs retained their ability to glide over the kinesin surface, albeit with a velocity (626 $\pm$ 67 nm/s) lower than that of the microtubules lacking antibodies on their surface (774 $\pm$ 32 nm/s for control MTs; 760 $\pm$ 56 nm/s for TCO-MTs) (Figure 2.4E). This effect on the gliding velocity is consistent with earlier reports of lowered gliding velocity of microtubules in the presence of "roadblocks" on their surface, although the decrease in the gliding velocity is not as drastic as was expected from those studies. The assembled Ab-MTs gliding over a surface of kinesin motors in the presence of ATP constituted the biosensing platform, where the antibodies conjugated to the microtubules surface can specifically detect analyte that has the complementary antigen on their surface.

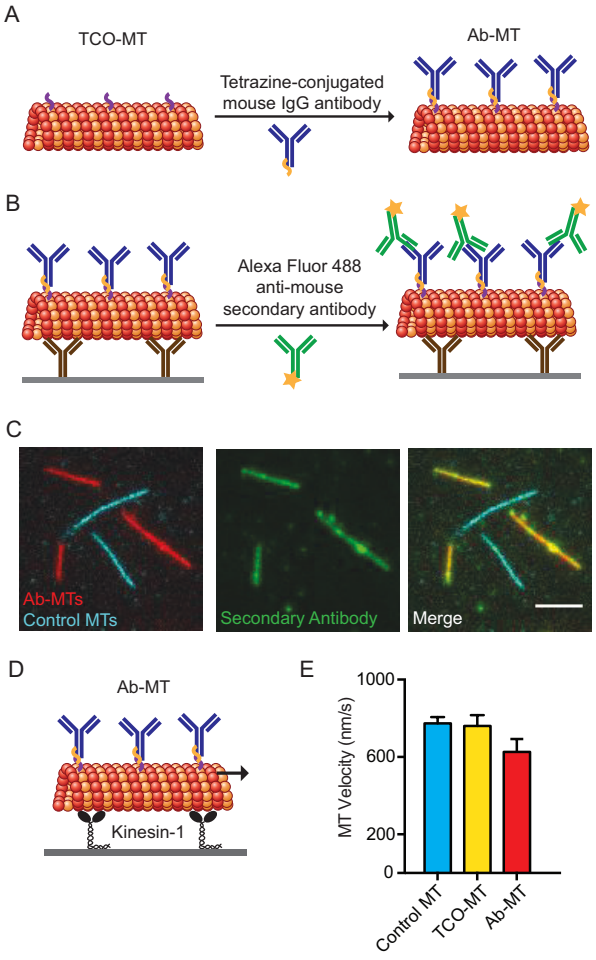

Figure 2.4: Covalent conjugation of antibodies to microtubules - A. *trans*-cyclooctene (TCO) conjugated microtubules (TCO-MT) were polymerized from TCO-tubulin, rhodamine-tubulin and unlabeled tubulin mixed in 4:1:3 ratio. Tetrazine-conjugated anti-CD45 mouse IgG antibodies were covalently coupled to the TCO-MTs *via* TCO-tetrazine bioorthogonal reaction, to generate antibody-conjugated microtubules (AB-MTs). (B, C) The Ab-MTs (red) and the control MTs (cyan) were immobilized on glass surface using anti-rhodamine antibodies. 100 nM fluorescent Alexa Fluor 488 anti-mouse secondary antibodies were added to these stationary microtubules, incubated for 30 min, and washed off. The specific co-localization of the fluorescent secondary antibody signal to the Ab-MTs, and not to the control MTs demonstrate successful conjugation of tetrazine antibodies to the TCO-MTs. Scale bar 5 µm. (D, E) The Ab-MTs, the TCO-MTs and the control MTs were used in a kinesin gliding motility assay. The gliding velocity (mean ± s.d.) of the Ab-MTs (626 ± 67 nm/s) was lower than that of the TCO-MTs (760 ± 56 nm/s) and the control-MTs (774 ± 32 nm/s).

2.3 Attachment of streptavidin to microtubules for roadblock studies

Streptavidin was modified using tetrazine-$(PEG)_5$-NHS and covalently conjugated to the TCO-MTs (Figure 2.5A) . Two types of fluorescent streptavidins were used to conjugate to microtubules - Alexa Fluor 647 Streptavidin and Fluorescein streptavidin.

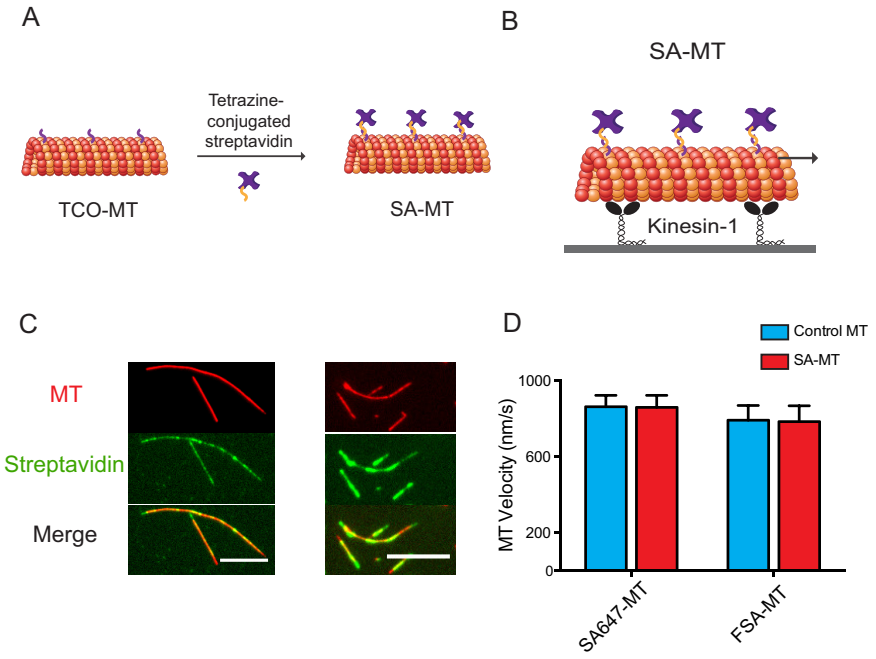

Figure 2.5: Covalent conjugation of streptavidin to microtubules - A. Tetrazine-conjuagted streptavidin was colavently conjugated to TCO-MTs using biorthogonal reaction. B. The streptavidin conjugated microtubules (SA-MTs) were then used in kinesin gliding motility assay. C. Fluorescence images of different streptavidin conjugated microtubules shows successful conjugation of the fluorescent streptavidins to the microtubules. D. Gliding velocities of the SA-MTs are similar to that of the control-microtubules.

The streptavidin-conjugated microtubules were then evaluated in a kinesin gliding motility assay (Figure 2.5B). Cy5 -labeled microtubules were used as control in the same assay. Specific co-localization of fluorescence signal from the streptavidin to the TCO-MTs confirmed successful conjugation (Figure 2.5C).

Surprisingly, the gliding velocity of the streptavidin conjugated microtubules (for both types of fluorescent streptavidins) was found to be similar that of the control microtubules that lacked any streptavidin on their surface (2.5D). This observation is in contrast with previous "roadblock" studies that showed conjugation of streptavidin to microtubules led to dramatic decrease in microtubule gliding velocity[85,86].

To explain this apparent discrepancy, it is important to understand the nature of the streptavidin-biotin interaction and how the streptavidin binds to the microtubules in these assays. Streptavidin is a homotetrameric protein that binds with exceptional affinity to the small biotin group (K_d $10^{-14}M$; strongest known non-covalent interaction)[89]. Structurally, streptavidin can be approximated as a cuboid of 5.4 nm x 5.8 nm x 4.8 nm dimension, with the biotin binding sites buried 1.7 nm or 1.9 nm (depending on the side) deep inside the streptavidin core[90–92] (Figure 2.6A). A key difference between the previously reported streptavidin-microtubule setups and the one developed in this thesis lies in the length of the linker separating the streptavidin from the microtubule surface. The previous setups used biotinylated microtubules in which the biotin was conjugated to the tubulin *via* an approximately 3.05 nm long spacer arm; the streptavidin would bind to these biotins on the microtubule surface. As the biotin binding sites are located roughly 2 nm inside the streptavidin core, this means that the effective distance at which the streptavidins were held from the microtubule surface in these assays was around 1 nm (Spacer arm - depth of biotin binding pocket; see Figure 2.6B (left)). In the assay used in this thesis, the streptavidin is covalently conjugated to the microtubules using a bioorthogonal reaction between tetrazine functionalized streptavidin and TCO-functionalized microtubule, each with 5 and 4 PEG units respectively (Figure 2.6B (right)). As a result, in this case, the distance at which the streptavidin is held from the microtubule surface is the sum of the lengths of the both the conjugating groups and their linkers (that is, TCO-$(PEG)_4$ + tetrazine-$(PEG)_5$), which is around 5-7 nm (from the structural information provided by vendors). The non-reduction of microtubule gliding velocity in the case where streptavidin cargo is held at this relatively longer distance indicates that the long linker attached to the cargo circumvents the "roadblock effect". Interestingly, this distance falls in the same range as the

dimensions of the kinesin motor head[93]. Attachment of cargo *via* a linker of comparable dimension or longer than the motor head can, therefore, facilitate the access of the kinesin motor heads to their binding sites on the microtubule even in the presence of a high density of the cargo. This explains the gliding velocity of the streptavidin-conjugated microtubules in the current setup. Additionally, this provides an explanation for the effect in gliding velocity observed in the previous section for antibody-conjugated microtubules assembled with the same bioorthogonal strategy. Antibodies (MW $\sim$ 150 kDa) are almost three times the size of streptavidin proteins (MW $\sim$ 50 kDa). So while the long linker does mitigate some of the roadblock effects, the large sized antibody-cargos offer more resistance than the streptavidins to the access of the kinesin motor head binding sites on the microtubules. As a result, the microtubule gliding velocity is decreased, although not to the same extent as would be expected from the previous reports where cargo was conjugated with very short linkers.

The covalently conjugated streptavidin to microtubules constitutes an excellent system for studying how different motors navigate obstacles *in vitro* on the microtubule surface. As different purified motor proteins often work optimally with different buffers, the covalently conjugated streptavidins can act as "permanent roadblocks" for biophysical characterization of motor movement in different buffer systems. From a biological perspective, these minimal reconstituted systems can offer understanding on how the motor proteins go around roadblocks in the highly crowded environment of the cell.

Additionally, as the covalent attachment of cargo to microtubules *via* long flexible linker leads to circumvention of the "roadblock effect", it it interesting to investigate the details of this phenomenon. In the next section, the effect of linker length on cargo attachment to microtubules is investigated by conjugating fluorescent streptavidin to microtubules *via* flexible PEG linkers of different lengths.

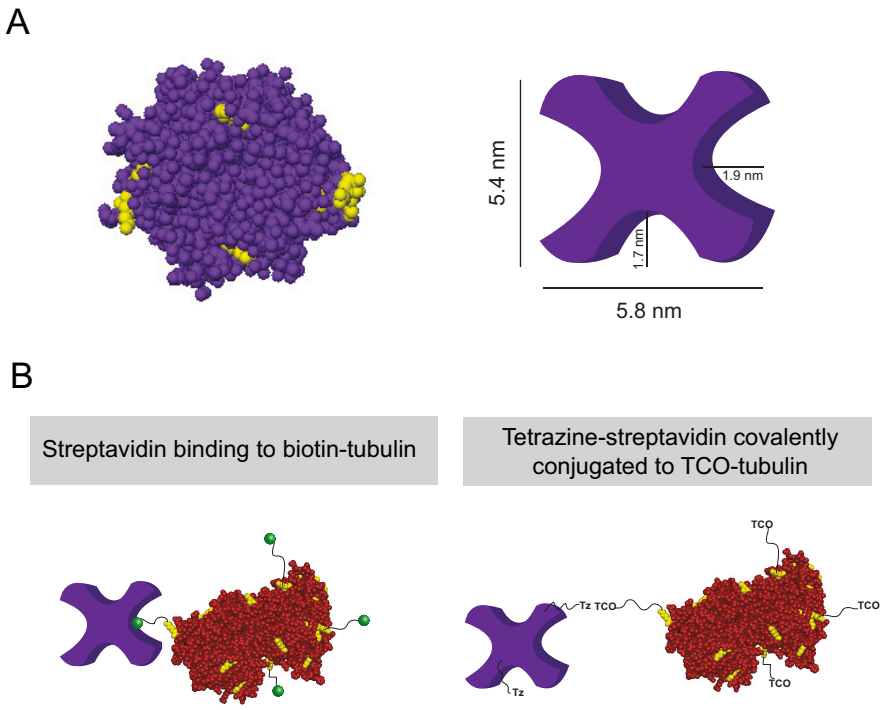

Figure 2.6: Streptavidin and its attachment to biotin-tubulin - A. Streptavidin is cuboid in shape with the biotin binding sites located 1.7 - 1.9 nm inside the protein. B. Attachment of streptavidin to biotin-tubulin (left) and covalent conjugation of tetrazine-streptavidin to TCO-tubulin (right).

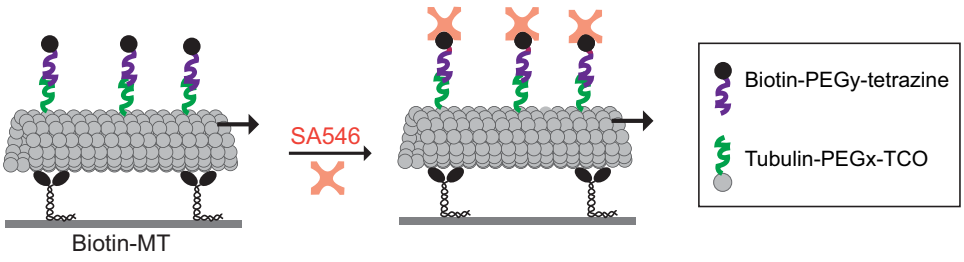

Figure 2.7: Scheme showing attachment of fluorescent streptavidin to biotinlyated microtubules in a gliding motility assay - Biotinylated microtubules were prepared by covalently conjugating tetrazine-Biotin-PEGy to TCO-PEGx-labeled microtubules. Fluorescent streptavidin was added to bind to these biotins attached *via* linker of $(x + y)$ PEG units on the microtubules.

2.4 Cargo attachment to microtubules *via* flexible linker circumvents the roadblock effect

Biotin-conjugated microtubules (Biotin-MT) were polymerized from a 4:1, 1:1, 1:4 mixture of TCO-$(PEG)_x$-tubulin (see section 2.1) and Alexa Fluor 488 tubulin, followed by incubation of these microtubules with Biotin-PEGy-tetrazine (x = 0, 4, 12; y = 0, 2, 4, 6). These Biotin-MTs (at 80%, 50%, and 20% biotinylation ratios) with various lengths of the PEG linker were then added to a kinesin gliding motility assay, along with control Cy5-microtubules. Alexa Fluor 546 Streptavidin (SA546) at 10 μM concentration was added to these microtubules, incubated for 10 minutes, followed by washing off of the excess, unbound SA546 (Figure 2.7). The amount of SA546 that binds to the Biotin-MT and the corresponding gliding velocity of these microtubules were quantified as a function of the total PEG linker length.

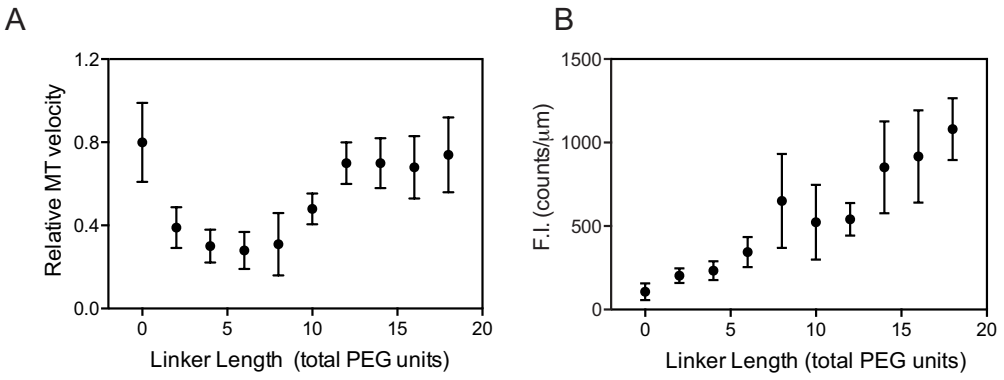

Figure 2.8: Microtubule gliding velocities and amount of fluorescent streptavidin loaded on 80% biotinylated microtubules for various linker lengths - A. Relative gliding velocity of streptavidin-loaded biotinylated microtubules as a function of the total PEG units in the linker. For 0 PEG units, the gliding velocity is unaffected. Thereafter, as the linker length increases, the relative gliding velocity of the microtubules also increase. B. Fluorescence intensity (F.I.) of the loaded streptavidin per unit length of microtubule as a function of the total PEG units in the linker (green) increases with the increase in the linker length. The relative gliding velocity data is plotted in grey for each data point (mean ± standard deviation).

Figure 2.8 shows the data evaluated from gliding motility assay with SA546 loaded Biotin-MTs at 80% biotinylation ratio (corresponding to the highest cargo density). Figure 2.8A shows the plot of the relative gliding velocity of the SA546 loaded Biotin-MTs *versus* the total PEG linker length. At 0 PEG units, the gliding velocity of the microtubules was similar to that of the control microtubules without the SA546 cargo. Thereafter, the relative microtubule velocity drops as the PEG units in the linker increases. However, after 6 PEG linker units, the relative gliding velocity of the cargo-conjugated microtubules increases, and plateaus off as the number of PEG units reaches 12. Figure 2.8B plots the fluorescence intensity (F.I.; green data) from the cargo (SA546) as a function of the linker length. In the background, the relative microtubule velocity as a function of the linker length is plotted in grey. The increase in the number of PEG units of the linker results in a corresponding increase in the F.I.. When the number of PEG units is 0, the very low F.I. shows that there is very less cargo loading in this case. The low amount of attached cargo is insufficient to have any significant roadblock effect, which explains why the microtubule gliding velocity is unaffected in the case of 0 linker unit. As the number of PEG units increase, the amount of cargo that gets attached increases linearly (linear fit $R^2 = 0.92$). Thus, the linker length of the cargo affects two aspects of the gliding motility assay: the amount of cargo attached (enhanced by increasing the linker length), and the transport velocity of the cargo-conjugated microtubules (increases with the linker length, expect for 0 linker length).Similar evaluations of the data obtained from gliding motility assay with SA conjugated Biotin-MTs at 50% and 20% biotinylation ratios are shown in Figure 2.9A and Figure 2.9B respectively. The observed trends were similar to that of the data-set at 80% biotinylation ratio.

Figure 2.10 shows the plot of F.I. versus linker length for all the data-sets. For each data point, the corresponding relative microtubule velocity is represented by a colour of the heat map. The blue, red, and yellow lines represent 80%, 50%, and 20% biotinylation ratios respectively. For a given biotinylation ratio, the amount of cargo attached increases with the increase in the linker length, as observed from the increase in F.I. values. For a given linker length, as the biotinylation ratio increases from 20% to 80%, there is a increase in the amount of cargo attached while the relative gliding velocity of the microtubules decreases. This trend was

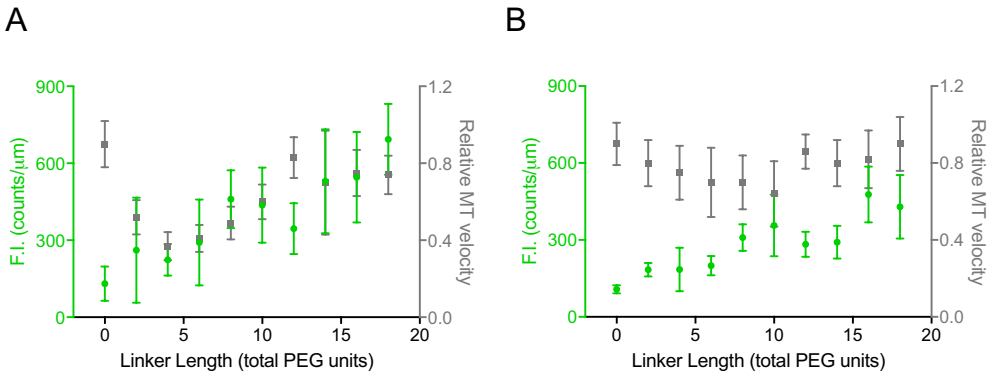

Figure 2.9: Microtubule gliding velocities and amount of fluorescent streptavidin loaded on 50% and 20% biotinylated microtubules for various linker lengths - Fluorescence intensity (F.I.) of the loaded streptavidin per unit length of microtubule (green data points) and the relative microtubule velocities (grey data points) plotted as a function of the total PEG units in the linker for 50% (A) and 20% (B) biotinylated microtubules (mean ± standard deviation).

found to be consistent across all linker lengths, except at 0 PEG units, at which the very low F.I. value indicates negligible cargo attachment with no observed effect on the gliding velocity at all three biotinylation ratios. This observation at 0 linker length can be explained as follows: the biotin binding sites are situated 1.7-1.9 nm deep inside the streptavidin core. For the biotin attached to the microtubules *via* linkers shorter than this length, the biotin is unable to access the binding sites within streptavidin, impairing successful binding of streptavidin to these biotinylated microtubules. As the linker length increases, the biotin can access these sites, and successfully bind to the streptavidin; this binding was enhanced with increased linker length. The long and flexible linkers offer greater degree of freedom to the biotin conjugated to the microtubules, allowing them to have better access, and subsequently better binding, to the biotin-binding sites inside the streptavidin.

The effect on microtubule gliding velocity for increased biotinylation ratios at a given linker length is consistent with the previous reports on the "roadblock effect", where increased amount of attached cargo on the microtubules leads to a corresponding decrease in the microtubule gliding velocity. However, it is interesting how this effect manifests with changes in the length of the linker *via*

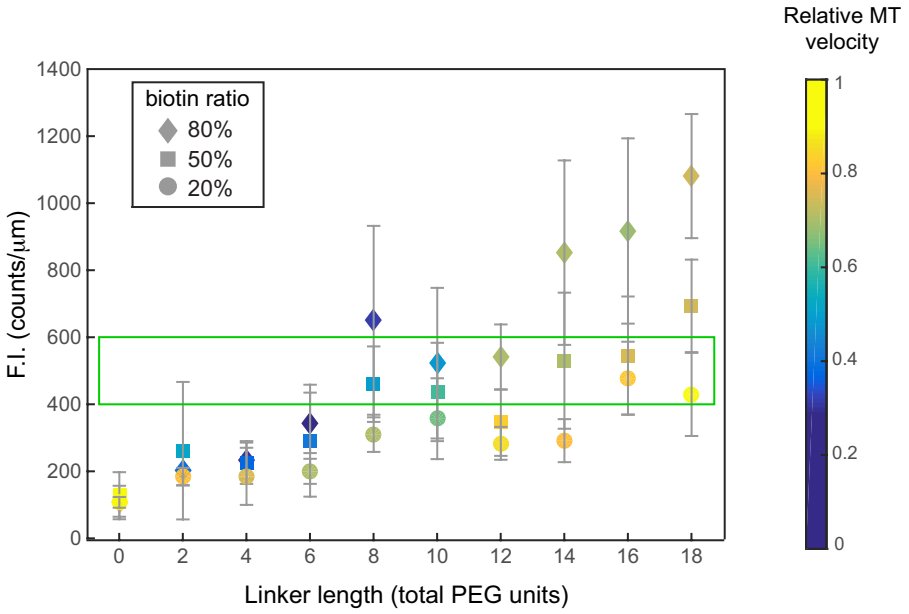

Figure 2.10: Combined plot of fluorescence intensity of the loaded streptavidin and relative microtubule gliding velocity as a function of the linker length - Fluorescence intensity (F.I.) of the loaded streptavidin per unit length of the microtubule is plotted (mean ± standard deviation) as a function of the linker length for all three microtubule biotinylation ratios. The diamond, square, and circle points corresponds to data from 80%, 50%, and 20% biotinylation ratios respectively. The relative gliding velocity of the microtubules is represented by a colour of the heat map (right of the graph). The green box shows all data points with similar amount of loaded streptavidin on the microtubules, corresponding to $400 - 600 counts/\mu m$ F.I. values.

which the cargo is attached to the microtubules. For linker length upto 10 PEG units, the relative microtubule gliding velocity decreases from around 80% to almost 20% of its initial velocity for increase in biotinylation ratio from 20% to 80%. For 2-10 PEG units in the linker length, a small increase in the cargo loading to the microtuble led to a drastic decrease in the gliding velocity. For cargo attached *via* linker with more than 10 PEG units, the decrease in gliding velocity with increased cargo loading was less dramatic. Going from 20% to 80% biotinylation ratio for $>$ 10 PEG units of linker length, the relative reduction in the gliding velocity decreased as the linker length increased. To put this in context, at 6 units of PEG linker, the relative gliding velocity decreased from $\sim$ 70% to $\sim$ 30% from 20% to 80% biotinylation ratio; at 18 units of the PEG linker, the velocity decreased from 90% to $\sim$ 75% for 20% and 80% biotinylation ratios respectively. Interestingly, the amount of cargo on the microtubules at 80% biotinylation ratio for the 18 unit linker was $>$ 3 times that on the microtubules for the 6 unit linker. The green box in Figure 2.10 shows the data for F.I. in the range of $400 - 600$ $counts/\mu m$. For this F.I range, that is, at similar amount of loaded cargo on the microtubules, as the linker length increases, the microtubules glide faster.

The total length of the linkers[94] can be estimated by multiplying the number of PEG units with the Kuhn length of PEG[95]. The 6 PEG units linker corresponds to a length of $\sim$ 4 nm, while that of 12 and 18 units are $\sim$ 8 nm and $\sim$ 12 nm respectively. As described above, it was from 12 units of linker length that the "roadblock effect" was increasingly circumvented. Interestingly, the dimensions of kinesin motor head are estimated to be around 8 nm[93], which is in the same range as that of the 12 unit PEG linker. Taken together, these results indicate that as the length of the linker becomes equal to or larger than the dimensions of the kinesin motor head, the access of the kinesin motor heads to their binding sites on the microtubule is facilitated despite the presence of a high-density of cargo. Thus, attachment of cargo *via* long flexible linker can effectively circumvent the "roadblock effect" while additionally enhancing the efficiency of cargo-loading to the microtubules.

2.5 Conclusion

In this chapter, a novel method of cargo conjugation to microtubules *in vitro* was presented. The method used the tetrazine-*trans*-cyclooctene reaction, the fastest known bioorthogonal reaction, to covalently conjugate cargos to microtubules. Antibodies were conjugated to the microtubules to develop biosensing platforms for detection of different analytes. Fluorescent streptavidin was conjugated to the microtubules to serve as "permanent roadblocks" for characterization of the behaviour of different motors on encountering obstacles. Moreover, by conjugating streptavidin cargo to microubules *via* flexible PEG linkers of different lengths, the effect of linker length on cargo attachment and transport were investigated. It was shown that increase in linker length enhances the cargo-loading on the microtubules, and that cargo attachment *via* long linker can effectively circumvent the "roadblock effect" to rescue the velocity of cargo-conjugated microtubules in gliding motility assay. These results advance the current understandings on the transport of cargo-conjugated microtubules by kinesin motors, and provide useful design principles for the choice of suitable linker for cargo attachment to microtubules. Additionally, the described conjugation scheme can be easily adapted for loading other types of cargos, as iEDDA reactions have been shown to be compatible with a wide range of biomolecules. Because the iEDDA chemistry is orthogonal to other "click chemistry" schemes, it will open new opportunities for the simultaneous and sequential assembly of multiple modular units to microtubules in gliding motility assays.

3

Analyte detection with antibody-conjugated microtubules in gliding motility assay

Lab-on-chip devices have emerged as promising miniaturized analysis systems for chemical and biological applications in the recent years. Development of cost-effective, small and portable *in vitro* diagnostics devices for the diagnosis and treatment of diseases is currently changing the landscape of healthcare delivery. In clinical diagnostics, miniaturization helps by reducing the amount of sample required, shortening the analysis time and allowing increased throughput and automation. Portability allows point-of-care diagnosis even in non-clinical setting, improving access to healthcare and personalization of treatment.

Microfluidics has been the strongest enabling technology for the development of these miniaturized devices. Over the last years, several microfluidics-based diagnostics solutions have become popular in the market, such as, the Micronics PanNAT Molecular Diagnostics System for nucleic acid based immunoassays[96], the Alere Triage Cardiac Panel for the diagnosis of acute myocardial infarction[?] , and Abbott's i-Stat handheld blood analyzer for the measurement of whole-blood composition[97]. The commercial microfluidic devices commonly require external pressure source to drive fluid flow - as the power of the pump to drive fluid

flow is inversely related to the volume of the fluid, this sets a practical limit on miniaturization of these devices.

To overcome this limitation of miniaturization and develop portable point-of-care devices working on very low sample volume, *in vitro* nanotechnological applications of biomolecular motor based devices have been explored in recent years. Biomolecular motors have evolved over millions of years to convert chemical energy of ATP to mechanical work with incredible efficiency. Reconstitution of the biomolecular motor based transport allows the fabrication of fast, miniaturized detection devices that are driven by the active transport of biomolecular motors, and therefore do not require any external pump to drive mass transport. In this chapter, the antibody-conjugated microtubule platform developed in the previous chapter (2) is used to develop biosensing applications. The first set of applications focuses on the detection of protein analytes using fluorescence microscopy. Thereafter, a label-free detection platform is developed that uses supramolecular self-assembly of the antibody-conjugated microtubules as read-out for analyte detection.

Publication Results from this chapter (section 3.2) have been submitted for publication as:*Label-free detection of microvesicles and proteins by the bundling of gliding microtubules.* Samata Chaudhuri, Till Korten, Slobodanka Korten, Gloria Milani, Tobia Lana, Geertruy te Kronnie, and Stefan Diez. Nano Letters (in review).

3.1 Fluorescence-based analyte detection

Development of analytical devices based on fluorescence offers several advantages, such as, high-resolution data acquisition using relatively inexpensive set-ups, availability of well-characterized fluorescent dyes, ability to provide information on molecular interactions and conformational dynamics. Fluorescence-based detection is therefore widely used in lab-on-chip biosensing devices.

A novel biosening platform was developed using the antibody-conjugated microtubules (see Chapter 2) for the detection of fluorescent analyte. The platform was then used for direct detection of fluorescent proteins (commercially available

fluorescent secondary antibodies) and for detection of cell-lysate derived fusion protein using a conventional double sandwich assay.

Detection of fluorescent protein analyte

Detection of fluorescent protein analyte was performed by using Ab-MTs in gliding motility assays (Figure 3.1A). Fluorescent Alexa Fluor 488 anti-mouse secondary antibodies were used as model protein analyte to specifically bind to the Ab-MTs. Using Total Internal Reflection Fluorescence (TIRF) microscopy, the protein analyte was found to specifically bind to - and to be transported by - the Ab-MTs. After a short incubation incubation time of 10 min, it was possible to detect the protein analyte at concentrations as low as 0.1 pM using microliter sample volumes (Figure 3.1B). In the current assay setup, 0.1 pM of the analyte corresponds to about 30,000 molecules in the volume of the flow channels, or an average of 3 molecules per field of view (about 80 μm × 80 μm). Analyte detection at this low concentration demonstrates the high sensitivity of the detection method. Analyte binding and transport was not observed with control microtubules that lacked the covalently-conjugated antibodies on their surface, confirming the selectivity of the method. Additionally, the sensitivity of the detection scheme was unaffected by the presence of equivalent concentrations of fluorescent Cy3 anti-rabbit secondary antibodies as background proteins (Figure 3.1C).

Detection of analyte by gliding Ab-MTs offers several advantages over methods based on surface-immobilized antibodies: firstly, active transport allows distinction of the specific transport of analyte bound to the gliding microtubules from background molecules unspecifically bound to the surfaces of the detection chambers. Secondly, as active transport obviates elaborate washing steps, the detection time can be significantly decreased and robust detection devices working with microliter sample volumes can be fabricated.

Detection of abl-bcr fusion protein from leukemia cell lysate

Chronic myeloid leukemia (CML) is characterized by the presence of Philadelphia chromosome, formed through reciprocal translocation of the ABL protocooncogene from chromosome 9 to the BCR gene on chromosome 22 in leukemia cancer cells.

3. ANALYTE DETECTION WITH ANTIBODY-CONJUGATED MICROTUBULES IN GLIDING MOTILITY ASSAY

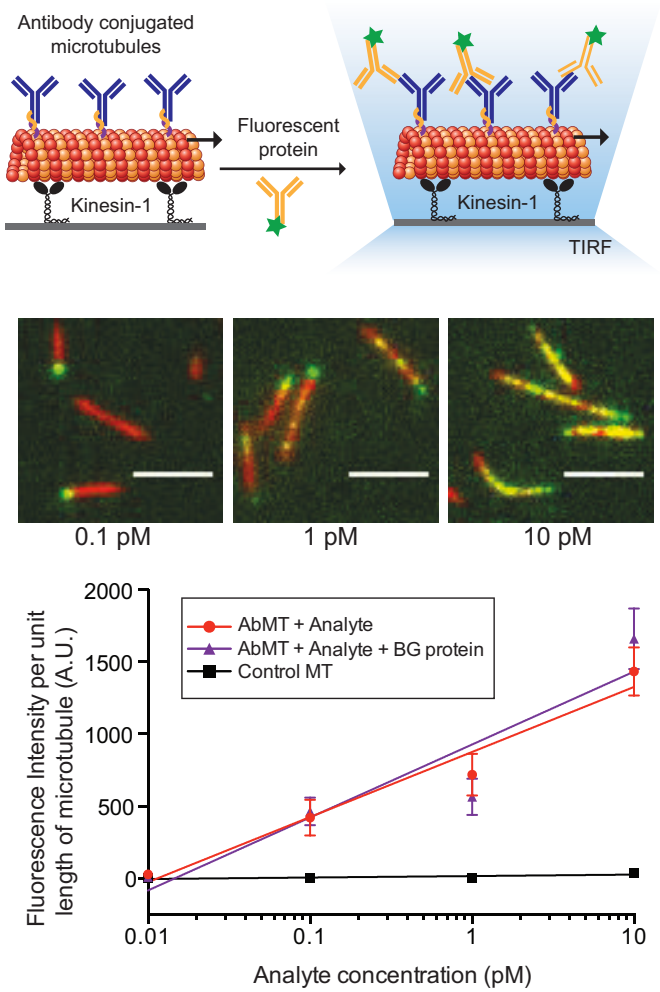

Figure 3.1: Detection of fluorescent protein analyte using Ab-MTs. - (A) Fluorescent protein analyte (Alexa Fluor 488 anti-mouse secondary antibodies) was detected by Ab-MTs in gliding motility assays using TIRF microscopy. (B) TIRF images of Ab-MTs (red) transporting fluorescent protein analyte (green) at 0.1 pM, 1 pM, and 10 pM concentrations. Scale bar 5 µm. (C) Plotting the increase in the fluorescence intensity of the analyte per unit length of Ab-MTs as function of analyte concentration demonstrates the sensitivity of the detection method down to 0.1 pM (red data). The sensitivity of the assay was not affected by the presence of equal concentrations of background fluorescent protein analyte (Cy3 anti-rabbit antibody; 'BG protein', blue line). Control microtubules without conjugated antibodies showed no increase in the fluorescence intensity upon addition of analyte (black line). For each data point, between 127 to 529 microtubules were analyzed (mean ± standard deviation). The detected signal on AbMTs at 0.1 pM analyte concentration was significantly different from that on the control MTs (Mann-Whitney U = 0, $p < 0.0001$).

The product of this fusion oncogene is a constitutively active tyrosine kinase (abl-bcr fusion protein), that results in activation of several signaling pathways leading to uncontrolled cellular proliferation and differentiation, and other characteristic symptoms of CML. This characteristic genetic signature and the expression of the abl-bcr fusion protein is a promising target for the development of diagnosis and treatment of CML.

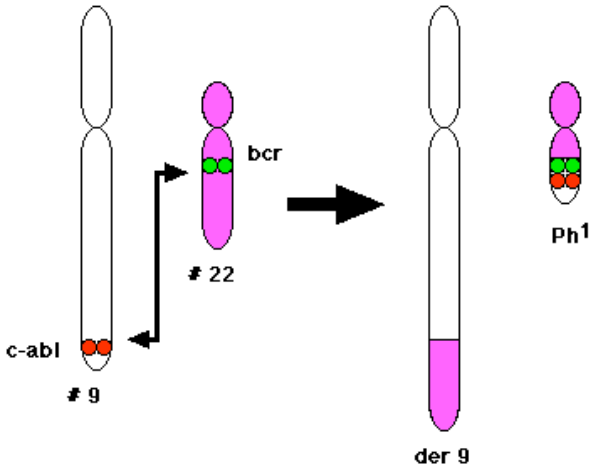

Figure 3.2: Schematic of reciprocal translocation in chronic myeloid leukemia (CML) - Schematic showing the reciprocal translocation between chromosome 9 and chromosome 22 resulting in the formation of an extra-long chromosome ("der 9") and the Philadelphia chromosome (Ph^1). The product of this Philadelphia chromosome is abl-bcr fusion protein, a biomarker for CML. Adapted from www.biology-pages.info[98]

Currently, diagnosis of CML is carried out by bone marrow biopsy, qualitative or quantitative PCR-based tests, and fluorescence *in situ* hybridization[99]. However, due the asymptomatic nature of the disease, patients with CML are mostly diagnosed at an advanced chronic stage of the disease in over 90% of the cases. Despite the high success rate of the current treatments for CML, this delayed diagnosis adversely affects on the prognosis and survival rates in patients. Development of fast, sensitive, simple and portable detection platform is therefore crucial for early diagnosis and treatment of CML.

As CML patients, even in the initial phase of the cancer, express the abl-bcr fusion protein in the cells of their bone marrow as well as peripheral blood[100],

detection of this fusion protein can enable early diagnosis of the disease, as well as assessment of the efficacy of various administered treatments. Here, a biosensing platform based on antibody-conjugated microtubules is developed for detection of abl-bcr fusion protein as a biomarker for CML diagnosis. The detection platform was built using by adapting the basic assay set-up described earlier 2.2. Anti-abl antibodies covalently conjugated to microtubules (Ab-MTs) using tetrazine-trans-cyclooctene bioorthogonal chemistry constituted the detector element. The following three cell lines were used for the experiments (Figure 3.3):

1. K652 Chronic Myeloid Leukemia cell line expressing CD45 surface antigen and the abl-bcr fusion protein

2. DND41 Acute Lymphocytic Leukemia cell line expressing the CD45 surface antigen but no fusion protein

3. MG63 Osteosarcoma cell line expressing neither the CD45 surface antigen nor the fusion protein

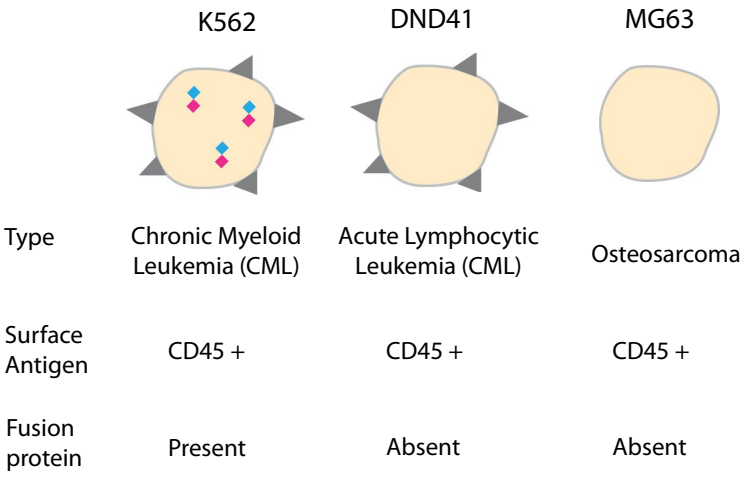

Figure 3.3: The cell lines used - K562, DND41, MG63

The cells from the above cell lines (Figure 3.3) were lysed, and the lysate added to antibody conjugated microtubules in gliding motility assay. Figure 3.4 shows the scheme of the detection assay. The detection platform consisted of anti-abl

goat IgG antibodies covalently conjugated to the microtubules (Abl-MTs) using trans-cyclooctene tetrazine bioorthogonal reaction. The abl-bcr fusion protein from the cell lysate would bind *via* the abl-binding site to the antibody conjugated microtubules. The detection of this fusion protein will be achieved using a double sandwich assay scheme, where monoclonal anti-bcr sheep IgG antibodies would bind to the bcr-moiety of the fusion protein, which would then be detected using fluorescent anti-sheep secondary antibodies.

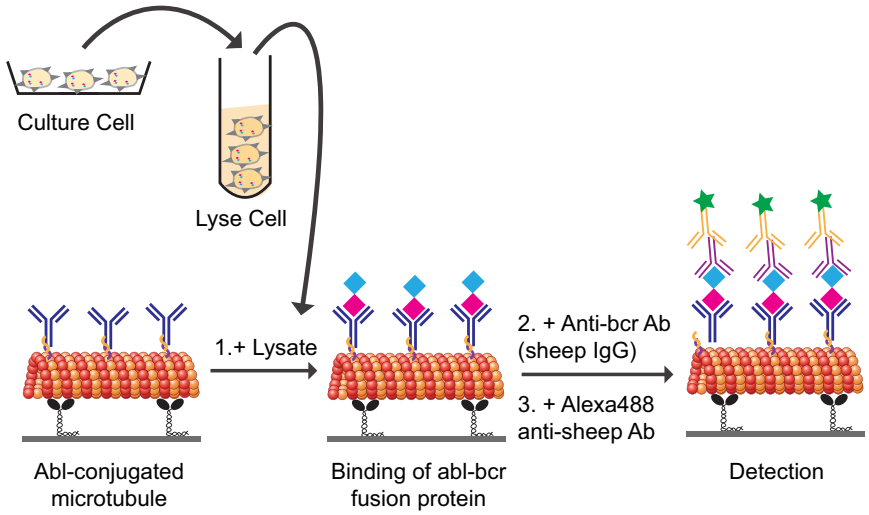

Figure 3.4: Abl-bcr fusion protein detection scheme 1. - The cell lysate was added to anti-abl antibody conjugated microtubules in a kinesin gliding motility assay. Successful capture of abl-bcr fusion protein from the cell lysate is confirmed by addition of monoclonal sheep IgG anti-bcr antibodies, followed by addition of fluorescent Alexa Fluor 488 anti-sheep secondary antibodies

Control experiment was first performed by adding the secondary anti-sheep antibodies to the Abl-MTs (anti abl antibody = goat IgG). The fluorescent anti-sheep secondary antibody was found to cross react with the monoclonal goat IgG on the microtubules, leading to a false positive in the absence of any fusion protein. As a result, this scheme was rendered unsuitable for detection of the abl-bcr fusion protein (Figure 3.5).

A modified approach was adopted for detection of the fusion protein. Here, instead of using a double-sandwich type of assay with fluorescent secondary antibodies, a direct detection scheme with fluorescently labeled antibody was

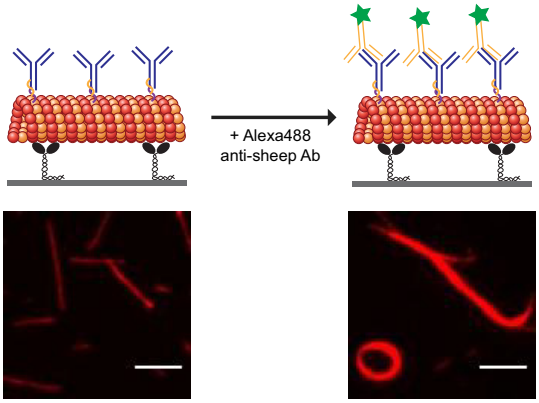

Figure 3.5: Control experiment with detection scheme 1 - Addition of Alexa Fluor 488 anti-sheep secondary antibodies to gliding abl(goat IgG)-conjugated microtubules led to bundling of the microtubules due to cross-reactivity of the anti-sheep secondary antibodies with the goat IgG antibodies on the microtubules. Scale bar 5 µm.

employed. The fusion protein from the cell lysate would bind to the Abl-MTs *via* the abl-fragment, and then be detected with fluorescent Alexa Fluor 488 labeled anti-bcr antibodies in the gliding motility assay.

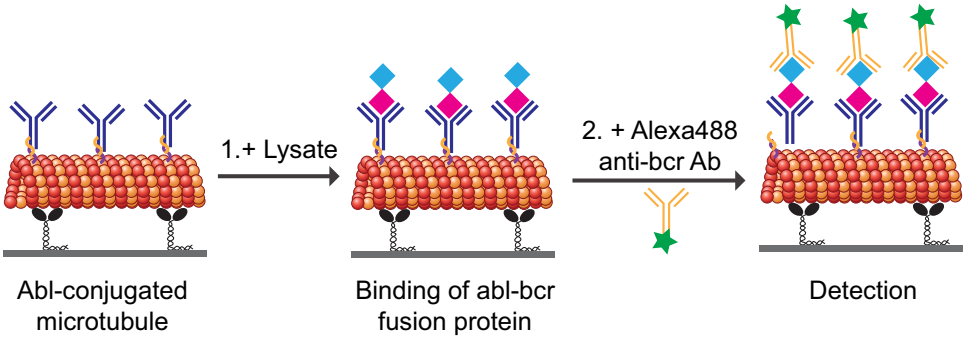

Figure 3.6: Abl-bcr fusion protein detection scheme 2 - Scheme - 1 (3.4) was modified to use fluorescent Alexa Fluor 488 anti-bcr antibodies for detection of the fusion protein in the second step

The cell lysate was obtained from the with 7000 cells/µl of the K562 (CML) cells and the DND41 (ALL, control) cells. Addition of the cell lysate led to decline in the gliding velocity of the microtubule as well as considerable microtubule bundling. The number of cells in the lysate was therefore diluted to

prepare lysate using 700 cell. At this concentration, the microtubule retained their normal motility. This observation is in line with the findings of Korten et al.[101], who reported that cell lysate obtained from a large number of cells (10000 cells/µl reported value) led to slow-down of the filaments and filament bundling for kinesin-microtubule gliding motility assays.

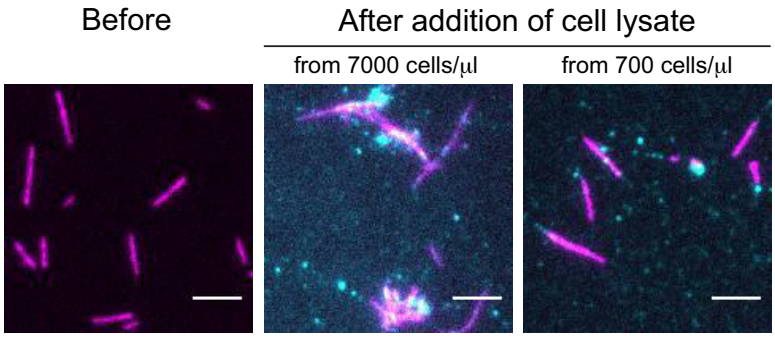

Figure 3.7: Effect of cell lysates on gliding microtubules. - Fluorescence images showing the abl-conjugated microtubules (magenta) before (left image) and after (middle and right image) addition of the cell lysate from K562 leukemia cells, followed by addition of Alexa Fluor 488 anti-bcr antibodies (cyan). The addition of cell lysate obtained from 7000 cells/µl led to microtubule aggregation (middle image), while the lysate obtained from 700 cells/µl did not affect the microtubule motility (right image). Scale bar 5 µm.

Following the addition of cell lysate from 700 cells/µl of K562, DND41 and MG63 cells to the Abl-MTs and subsequent addition of Alexa Fluor 488 anti-bcr antibodies, the fluorescence signal from the anti-bcr antibodies on the Abl-MTs was quantified. Figure 3.8 shows the fluorescence signal (per unit length of microtubule) from the anti-bcr antibodies on the Abl-MTs and the control microtubules (Ctrl-MT, without any antibody conjugated to the surface) after the addition, incubation, and washing off the cell-lysate from the three cell lines. The fluorescence intensity due the the K562 cell lysate was found to be significantly higher than that observed on addition of the cell lysate from either the MG63 or the DND41 cells. The fluorescence intensity due to the MG63 and DND41 cell lysate was comparable to that observed due to binding of the Alexa Fluor 488 anti-bcr antibodies in the absence of any cell lysate. A cut-off value set using the mean intensity $\pm$ 5 $\times$ standard deviation due to the negative control (no

cell lysate, only Alexa Fluor 488 anti-bcr antibodies added to gliding Abl-MTs) allowed clear distinction of signal due to the K562 lysate from that due to the control MG63 and DND41 cell lysates.

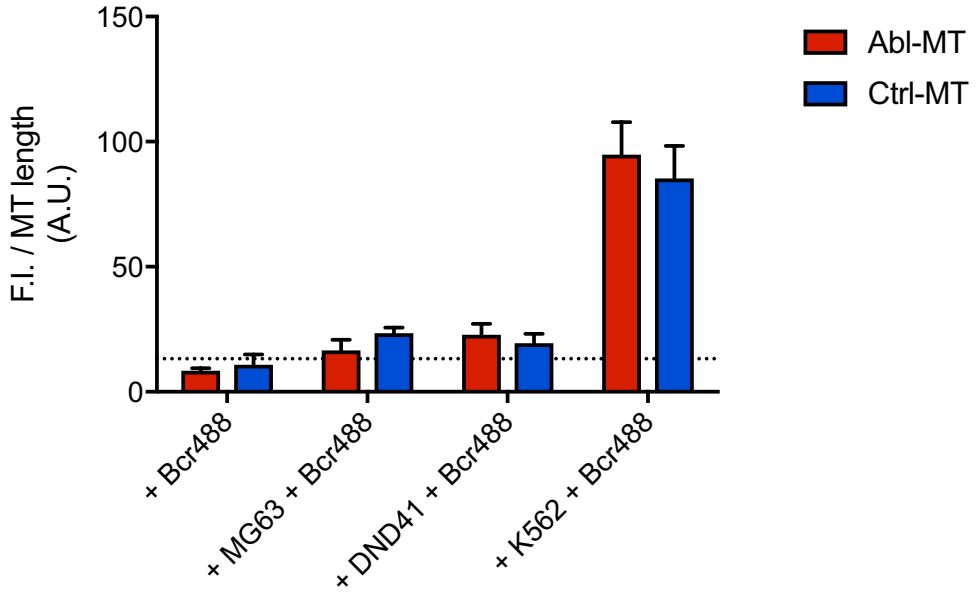

Figure 3.8: Detection of fusion protein from Chronic Myeloid Leukemia (CML) Cell line. - The fusion protein was detected by quantifying the fluorescence signal per unit length of the microtubules from the Alexa Fluor 488 anti-bcr antibodies using TIRF microscopy. The blue bars corresponds to the signal detected from the control microtubules, while the red bars indicate the signal detected from the Abl-MTs. The dotted line corresponds to mean ± standard deviation from the negative control (no cell lysate, only Alexa Fluor 488 anti-bcr antibodies added to the gliding Abl-MTs). Addition of cell lysate from the K652 CML cell line results in significant increase in signal, observed from both the Abl-MTs as well as the control microtubules.

Interestingly, both the Abl-MT as well as the control-microtubules displayed similar increase in the fluorescence signal on addition of the K562 cell lysate. This indicates that while the fusion protein binds to the Abl-MTs, the control microtubules also manage to capture the fusion protein or some other component from the lysate that is later recognized by the anti-bcr antibodies. Following up on this perplexing result led to a previous work by Miroshnychenko et al. [102], who

showed that pleckstrin homology domain from abl-bcr fusion protein has a very specific and high binding affinity to β tubulin. This study provides an explanation for the result obtained - the fusion protein binds to the anti-abl antibodies on the Abl-MTs, as well as to the β tubulin of the control microtubules, and is later recognized and quantified by the Alexa Fluor 488 anti-bcr antibody. This serendipitious result underscores the potential application of a standard gliding motility assay for the detection of abl-bcr for the diagnosis of CML.

3.2 Label-free analyte detection

Analyte detection is crucial for applications in healthcare[103,104], environmental and food safety[105], and drug discovery[106]. Thereby, the development of fast and sensitive label-free detection methods is becoming increasingly important as analyte labeling, besides being labor-intensive, expensive and time-consuming, often compromises the results[107,108]. Label-free detection contributes to fidelity and robustness of the assay. However, so far, most of the available label-free detection methods are based on surface reactions, often lacking the desired sensitivity and speed[109,110].

To overcome these limitations, a label-free detection platform was developed based on the self-assembly of antibody-conjugated microtubules (Ab-MTs) in a kinesin gliding motility assay. Owing to their small size, energy efficiency, and robustness in synthetic environments, biomolecular motors (like kinesin) and their associated cytoskeletal filaments (like microtubules) are an attractive choice for a wide range of nanotechnological applications[45,79–81]. Over the past decades, the biomolecular motors and their associated filaments have been extensively used for developing molecular sorting[3,7,9,11,111], surface imaging[44], and biosensing[6,10,87] devices. Around the same time, considerable research has been focused on studying the dynamic self-assembly (bundling and spooling) of cytoskeletal filaments, driven by active transport of biomolecular motors, that leads to the formation of highly ordered supramolecular structures *in vitro*[48,49]. While these latter studies aimed at understanding and tuning the mechanism of biomolecular motor driven self-assembly process[112–115], engineering applications with this phenomenon has not yet been reported.

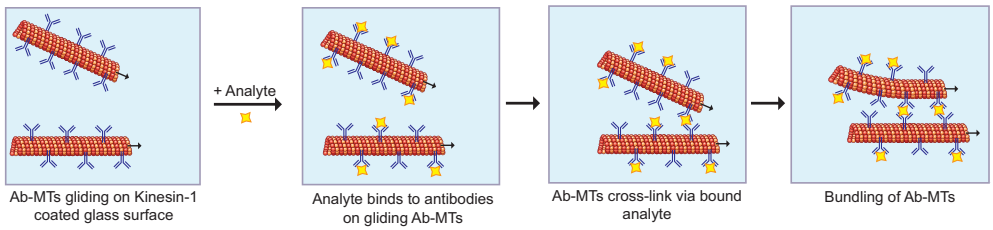

Figure 3.9: Scheme showing label-free detection of multivalent analyte. - Antibody conjugated microtubules (Ab-MTs) assemble to supramolecular assemblies of bundles and spools due to binding of the multivalent analyte.

Here, the Ab-MTs gliding over surface immobilized kinesin motors were used for the label-free detection of multivalent analytes (Figure 1). The antibodies on the gliding Ab-MTs capture the analyte by binding to their antigenic sites. For a multivalent analyte, each analyte molecule can bind to multiple Ab-MTs, thereby cross-linking them. In a motor-driven gliding motility assay, this results in the formation of supramolecular bundles and spools of Ab-MTs. This behavior of the gliding Ab-MTs upon addition of multivalent analytes enables the label-free detection of the analyte through characterization of Ab-MT bundling. Utilizing this phenomenon. the label-free detection of microvesicles and multivalent proteins was demonstrated, and the cross-reactivity between secondary antibodies was profiled. This reported method combines the inherent advantages of biomolecular motors for nanoscale transport with the motor-driven self-assembly of cytoskeletal filaments to successfully engineer a label-free biosensor for analyte detection.

Label-free detection of microvesicles as biomarker for acute lymphocytic leukemia

Microvesicles (MVs) are membrane-bound sacs with size of 50 nm to 1000 nm shed from almost all cells. The MVs reflect the antigenic and molecular content of the cells of origin, with a vital role in cell-to-cell communication as vehicles of biological information between cells under both normal and pathological conditions[116,117]. In recent years, there has been a growing interest in characterizing MVs as biomarker for various diseases and developing diagnostic devices based

on MV detection[118–120]. However, successful detection and development of effective diagnostic platforms with MVs remain challenging due to the requirements of extensive sample preparation and labeling steps[118,121]. To overcome these challenges, a biomolecular motor based MV detection platform was developed by using Ab-MTs in a gliding motility assay. As models, two different human cell lines were used – an acute lymphocytic leukemia (ALL) patient-derived human T-cell line (DND41, leukemia cell line) and a human osteosarcoma cell line (MG63, control cell line). The leukemia cells have hematopoietic marker CD45 antigens on their surface, while the control osteosarcoma cells lack these surface antigens[120]. Consequently, the leukemia cells and the control cells release CD45+ MVs (leukemia-MVs) and CD45- MVs (control-MVs), respectively.

MVs were isolated from 1000 cells/µl of the leukemia and the control cells (method detailed in section 6.4). A schematic of the assay is shown in Figure 3.10A. On addition of the leukemia MVs, the gliding Ab-MTs slowed down, and on encountering other Ab-MTs, assembled into bundles and spools, which continued adding more Ab-MTs units, propagating the dynamic self-assembly process. Fluorescent labeling of the cell lines prior to MV isolation yielded fluorescently labeled MVs, and the fluorescent signal from leukemia MVs was found to colocalize with that from the supramolecular Ab-MT assemblies. Control microtubules without antibodies conjugated to their surface showed no such self-assembly phenomenon on addition of the leukemia MVs and continued gliding without any change in their velocity. Additionally, no change in Ab-MT gliding was observed on addition of the control MVs, which did not show any colocalization with the Ab-MT either, confirming the specificity of the detection method (Figure 3.10B).

As the single Ab-MTs assembled into bundles on addition of the leukemia MVs, there was a corresponding increase in fluorescence intensity. Thus, by monitoring this increase in fluorescence intensity of the Ab-MTs, microtubule bundling due to the added analyte could be followed. The bundling process was quantified by monitoring the increase in fluorescence intensity of the Ab-MT assemblies. Median of the top 1% of the Ab-MT intensities (referred to from now on as fluorescence intensity or F.I.) in the field-of-view (FOV) was measured for several FOVs (30-40 FOVs) for 30 min after addition of the analyte. As the analyte causes the single

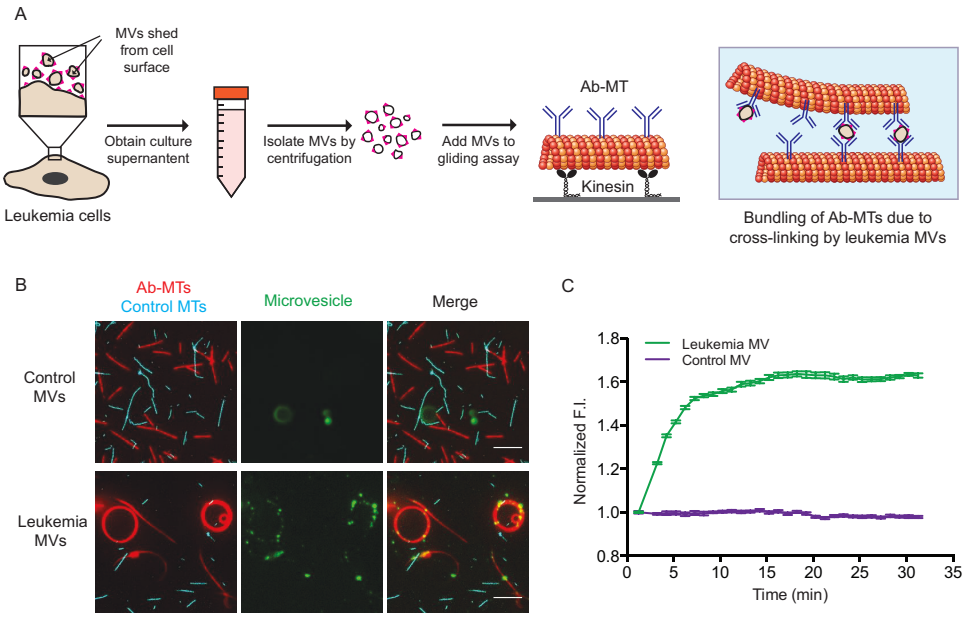

Figure 3.10: Label-free detection of microvesicles (MVs) as biomarker for acute lymphocytic leukemia (ALL). - (A) Schematic showing the workflow of MV detection. Leukemia MVs and control MVs were isolated by serial centrifugation from the supernatant of the cell culture of acute lymphocytic leukemia cells and osteosarcoma cells. The purified MVs were added directly to a gliding motility assay consisting of Ab-MTs and control MTs. The leukemia MVs cross-link the gliding Ab-MTs, causing the latter to bundle into supramolecular assemblies. This characteristic bundle and spool formation of the Ab-MTs on analyte addition is used as read-out for label-free analyte detection. (B) Fluorescence images of rhodamine labeled Ab-MTs (red) and Cy5-labeled control MTs (cyan) after addition of the labeled MVs (green). Addition of control MVs to assay does not affect the gliding of either the Ab-MTs or the control MTs. Addition of the leukemia MVs lead to the formation of large supramolecular assemblies of Ab-MT bundles and spools. This bundling process due to the leukemia MVs is specific; the control MTs continue gliding unaffected in the presence of the MVs. Fluorescent labeling of the cell lines prior to MV isolation yielded fluorescently labeled MVs. Exclusive co-localization of the fluorescence signal from the leukemia MVs to the Ab-MTs, and not the control-MTs further confirm the specificity of the detection. Scale bar 20 µm. (C) Plot of normalized F.I. of the Ab-MTs with time on addition of the leukemia MVs (green line) and the control MVs (purple line) shows characteristic increase in F.I. only for the leukemia curve.

Ab-MTs to assemble to bundles, the intensity histogram of the fluorescent Ab-MTs shifts towards a higher value. A plot of normalized F.I. versus time of the Ab-MTs after addition of the leukemia MVs and control MVs is shown in Figure 3.10C. While there was no change in the F.I. values of the Ab-MTs on addition of the control MVs, that of the Ab-MTs rapidly increase on addition of the leukemia MVs and eventually plateaus off. This distinct bundling profile of the Ab-MTs was used as read-out for the detection of the analyte. As the detection method is based on quantification of the signal from the self-assembly of Ab-MTs, it obviates the need to label the analyte, allowing label-free detection of the latter.

This example demonstrates the proof-of-principle application of the detection platform in future lab-on-chip devices for leukemia diagnosis. The method circumvents the need to label the isolated MVs, overcoming a key setback in development of MV based detection methods. Moreover, as the detection principle is based on molecular recognition between antigen and antibody, the biosensing platform can be easily adapted for MV-based diagnostic assessment of other medical conditions. The portability and ease of detection with the method is promising for the development of future, point-of-care MV detection.

Label-free, sub-nanomolar protein detection using the Ab-MT bundling as read-out

Dynamic self-assembly of gliding microtubules has been described earlier with biotinylated microtubules cross-linked by streptavidin[48,49]. Here we show that such self assembly process can also be brought about by any multivalent entity that can bind to specific sites (e.g. biotin or antibody) on the MTs. To explore further applications based on this phenomenon, the Ab-MT biosensing platform was used for label-free detection of proteins.

Alexa Fluor 488 anti-mouse secondary antibodies were used as model protein analyte to bind specifically to the mouse IgG antibodies on the surface of the Ab-MTs. Addition of the protein analyte led to similar read out as on addition of the leukemia MVs, i.e. rapid decline in gliding velocity and formation of characteristic large supramolecular assemblies of Ab-MT bundles. Control microtubules without antibodies conjugated to their surface showed no such self-assembly phenomena

3. ANALYTE DETECTION WITH ANTIBODY-CONJUGATED MICROTUBULES IN GLIDING MOTILITY ASSAY

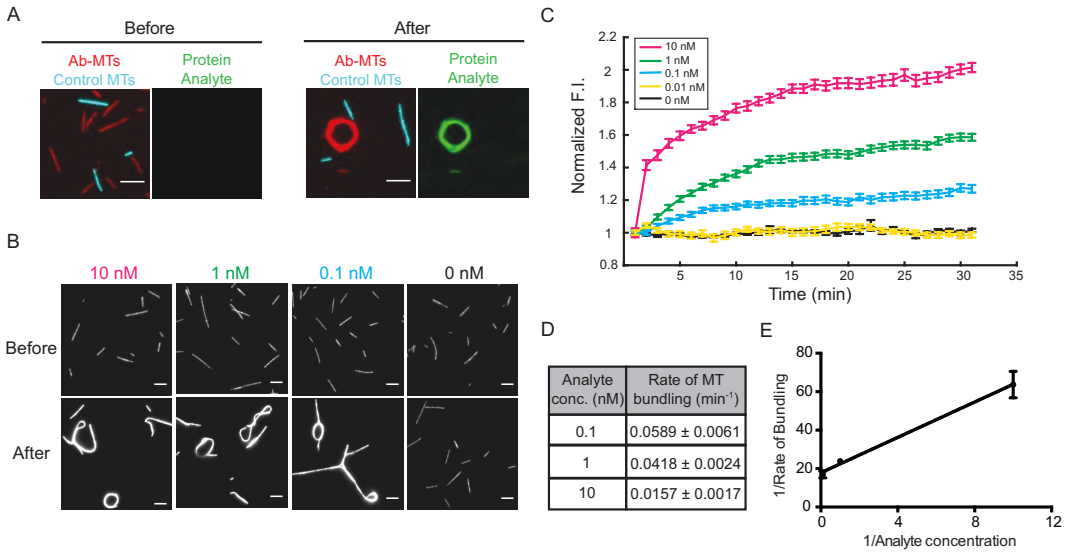

Figure 3.11: Label-free protein detection and profiling of antibody cross-reactivity - (A) Fluorescent images of Ab-MTs and control-MTs before and after addition of 10 nM model protein analyte. Addition of the specific protein analyte led to bundling and spooling of the Ab-MTs, but not of the control MTs. As the analyte used here was fluorescent Alexa Fluor 488 anti-mouse secondary antibody, exclusive co-localization of the fluorescent signal from the analyte to the Ab-MT assemblies confirms the specificity of the detection method. Scale bar 5 µm. (B) Fluorescence images of rhodamine labeled Ab-MTs in kinesin gliding motility assay before and after addition of the model protein analyte. The characteristic bundle and spool formation of the Ab-MTs on addition of the analyte was observed from 10 nM to 0.1 nM analyte concentrations. Scale bar 5 µm. (C) Plot of normalized F.I versus time for the Ab-MTs after addition of different concentration of the protein analyte. By fitting a second order polynomial to the curve obtained, the rate of bundling of the Ab-MTs was estimated from the slope of the curve at t = 0 for the protein analyte concentration of 10 nM, 1 nM and 0.1 nM (D) The rate of bundling for various concentrations of the protein analyte. (E) The reciprocal plot of the rate of Ab-MT bundling versus analyte concentration shows a linear dependence.

on addition of the analyte and continued gliding without any change in their velocity. As the analyte used here was fluorescent as well, observation of specific co-localization of the signal from the analyte to the Ab-MTs, and not to the control microtubules confirms the specificity of the detection method (Figure 3.11A).

Next, the sensitivity of label-free protein detection with the Ab-MT biosensors was investigated. Rapid and specific bundling of Ab-MTs was observed on analyte addition over a wide range of concentrations (Figure 3.11B). By quantifying the rate of increase in F.I. as a measure of the rate of Ab-MT bundling, the concentration of the added analyte could be determined (Figures 3.11C-E). The distinct bundling profile of the various analyte concentrations tested allows the label-free protein detection method to be quantitative, with sensitivity down to 0.1 nM concentration.

Thus, a simple, fast and robust method for label-free protein detection with sub-nanomolar sensitivity was successfully developed. The versatility of the method lies in the fact that by changing the antibody conjugated to the surface of the Ab-MT biosensing element, the platform can be easily adapted for detection of a wide range of analyte.

Profiling antibody cross-reactivity

Antibodies recognize and bind to specific regions on the antigen surface called epitope. However, in practice, antibodies can bind to similar sequence present on other antigens, leading to undesired cross-reactivity. Despite the widespread use of antibodies in biological research, diagnostics and therapeutics, cross-reactivity of antibodies poses a serious problem[122]. Evaluation of antibody cross reactivity is therefore crucial for any antibody-based application.

Here, cross reactivity between various secondary antibodies to monoclonal mouse antibody (human anti-CD45 mouse IgG antibody) present on the surface of the Ab-MTs was investigated. Secondary antibodies are commonly used in biochemical assays like Western blotting, flow cytometry, immunohistochemistry, and cross reactivity between secondary antibodies can compromise the assay results. The following commercially available secondary antibodies were tested

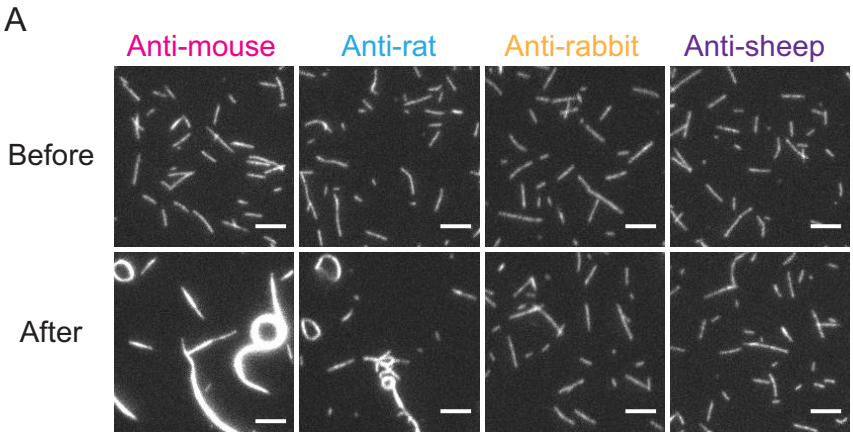

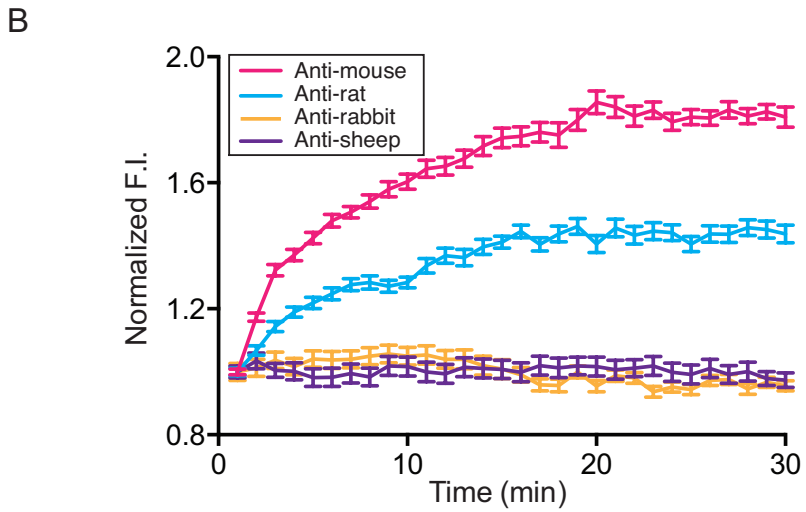

Analyte conc. (nM)	Anti-mouse	Anti-rat
Rate of MT bundling (min^{-1})	0.0630 ± 0.0036	0.0371 ± 0.0021

Figure 3.12: Profiling antibody cross reactivity. - (A) Fluorescent images of rhodamine labeled Ab-MTs before and after addition of 10 nM of various secondary antibodies (anti-mouse, anti-rat, anti-rabbit and anti-sheep secondary antibodies). Addition of anti-mouse secondary antibodies led to the characteristic bundling of the Ab-MTs, which have monoclonal mouse IgG on their surface. However, cross-reactivity between anti-rat secondary antibodies and mouse IgG on Ab-MTs also led to the formation of bundles and spools of Ab-MTs. No cross-reactivity between anti-rabbit and anti-sheep secondary antibodies was observed with the mouse IgG on the Ab-MTs. Scale bar 5 µm. (B) The cross-reactivity between various secondary antibodies with mouse IgG on the Ab-MTs can be estimated by plotting the normalized F.I. of the Ab-MTs with time. By obtaining the rate of bundling of the Ab-MTs due to the secondary antibody, the secondary antibody cross reactivity can be estimated.

for their propensity to bind to mouse monoclonal antibody: anti-mouse, anti-rat, anti-goat and anti-sheep antibodies.

Each of the secondary antibodies at 10 nM concentration was added to the Ab-MTs in kinesin gliding motility assay (Figure 3.12A). Addition of the anti-mouse secondary antibodies led to rapid bundling of the Ab-MTs, as expected. Addition of 10 nM of anti-rat secondary antibodies also led to Ab-MT self-assembly and bundling; no such self-assembly process was observed on addition of anti-goat or anti-sheep secondary antibodies at the same concentration. By quantifying the rate of Ab-MT bundling, the extent of cross-reactivity of these secondary antibodies with monoclonal mouse antibodies could be estimated (Figure 3.12B). The rate of bundling was found to be 0.0630 ± 0.0036 min^{-1} and 0.0371 ± 0.0031 min^{-1} with 10 nM anti-mouse and anti-rat antibodies respectively, while no bundling was observed for the anti-goat and anti-sheep antibodies. Given the closeness at species level between mouse and rat, the degree of cross-reactivity of anti-rat secondary antibodies to mouse IgG antibodies can be explained. Thus, using bundling of Ab-MTs as a read-out, successful application of the developed biosensing platform was demonstrated as a tool for rapid profiling of antibody cross reactivity.

3.3 Conclusion

In this chapter, a biosensing platform for analyte detection was developed by covalently conjugating antibodies to microtubule using the tetrazine-*trans*-cyclooctene iEDDA reaction established previously in chapter 2. Two types of analyte-detection schemes were employed - fluorescence-based analyte detection and label-free analyte detection. In the first scheme, highly sensitive, sub-picomolar detection of fluorescent protein was demonstrated with the gliding antibody-conjugated microtubules. Next, a label-free detection method was demonstrated by quantifying the read-out of microtubule bundling in the presence of specific analyte. The label-free detection platform was used to specifically detect microvesicles as biomarkers for leukemia diagnosis. Additionally, the versatility of the label-free method was demonstrated by profiling cross-reactivity between commercially available secondary antibodies. Since the biorecognition principle of the developed detection platform is based on molecular recognition between antigen and antibody, the

assay is easily amenable to be used for the detection of a wide range of analytes with known and available antibodies or other capture agents such as aptamers. With the variety of commercially available antibodies and the ongoing research on identifying microvesicles for cancer diagnosis, the reported method paves way for the development of fast and sensitive detection platform for point-of-care diagnosis of various diseases.

4

Microtubule gliding in nanostructures

An important criterion for efficient transport is successful control over the transport directionality. Although *in vitro* reconstitution microtubule transport by biomolecular motors have been established in the last few decades, the field of nanotechnological applications of biomolecular motors still faces the challenge of achieving controlled, unidirectional transport. As most of the nanotechnological applications employ the gliding motility assay geometry, considerable research effort has been directed over the years at controlling the microtubule gliding motility, such as by using chemical pattering or topographical structures (detailed in the section 1.2). A combination of both these methods, where the motor proteins are specifically restricted through differential surface chemistry to the bottom of trenches in topographical structures, has proven to be most successful[9,72,77,123,124].

The ease of fabrication and design flexibility offered by the topographical structures has led to the development of several applications including fabrication of molecular sorting devices for protein concentration[9,74], and parallel biocomputation network based on lithographic patterning[124]. While the lithographic microstructures provide a promising means of controlling microtubule motility through physical confinement, robust assay performance in these surfaces is critical for the development of more challenging applications with biomolecular motors. Low quality of gliding motility assay on these structures due to reduced microtubule landing, increased microtubule detachment, and frequent impairment of

motility due to stuck microtubules currently limits the practical applicability of these structures[66,69,74].

Previous studies have focused on understanding how the structural design of the nanostructures affect the quality of microtubule motility. While these studies led to the design of structures with improved microtubule guiding, all these studies employed the standard gliding motility assay as used on glass surface, and do not address the issues arising out of variability in the basic assay set-up. To further implementation of these structures, it is important to understand how the basic assay components, such as the type of kinesin or microtubule stabilization method affects the assay performance.

Here, gliding motility under different assay conditions on the nanofabricated chips will be characterized to develop an optimized assay protocol for improved gliding motility assay on these lithographic nanostructures. Following the optimization of assay protocol for the nanostructures, a lab-on-chip concentrator device to effectively guide and direct the microtubule motility is developed. Based on previous design of lithographically patterned structures to rectify and control microtubule motility *in vitro*[123], the nanostructured device aims at achieving a concentration effect that can improve the detection limit in microtubule-motor based biosensing applications. The efficiency of this concentrator effect is evaluated and a potential application demonstrated using leukemia-cell derived microvesicle transport and concentration in the devices.

Publication Results from this chapter (section 4.1) have been included in: *Kinesin-1 expressed in insect-cells improves microtubule in vitro gliding performance, long-term stability and guiding efficiency in nanostructures.* T. Korten, S. Chaudhuri, E. Tavkin, M. Braun, and S. Diez. IEEE Transactions on NanoBioscience, 15(1), 62-69 (2016).

4.1 Characterization of microtubule gliding in nanostructures

A combination of nanofabrication process and chemical adsorption, similar to the one described earlier[123], was used to design the chips (details of the fabrication process in section 6.5). The structures consisted of a gold (Au) floor surrounded by 500 nm high glass boundary walls. The glass walls were coated with PEG-silane, followed by kinesin immobilization on the gold surface. This restricted microtubule motility only on the Au surface, with the delineating PEGylated walls acting as physical confinements guiding the microtubule movement.

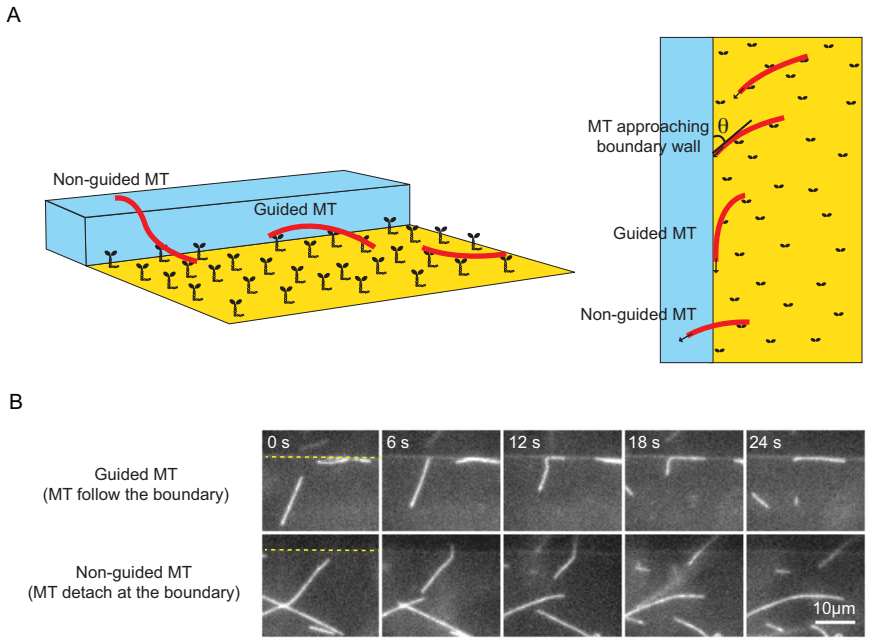

Figure 4.1: Microtubule guiding by the topographical structure. - A. The gliding microtubules on reaching the PEGylated boundary wall can either be guided to continue gliding in the Au channel (guided MT), or can escape the channel by crossing the boundary or detaching (non-guided MT). B. Fluorescence images of rhodamine labeled microtubules being guided (top row), or detaching (bottom row) on approaching the boundary wall.

Microtubule gliding was restricted only to the gold surface, with no gliding observed on the glass surfaces. This can be attributed to the protein-repellant

PEG coating of the glass surfaces, which prevent the binding of kinesin and subsequent motility of the microtubules.

To characterize motility on the nanostructures, the efficiency of guiding the microtubules within the channel design was evaluated (Figure 4.1). The approach angle, θ, of the microtubule was calculated relative to the boundary as shown in Figure. An event was classified as a guiding event if the microtubule oriented itself with the boundary wall and continued gliding within the channel. A non-guiding event was defined when the microtubule approaching the boundary wall detached from the surface, or climbed up the boundary wall to move into the PEGylated region. The data was binned in histogram with 15° intervals. The guiding efficiency was calculated as a ratio of guiding events to the total number of events (guiding and non-guiding) for a given range of approach angles:

$$E = \frac{N_{guided}}{N_{tot}} \tag{4.1}$$

where E is the guiding efficiency, N_{guided} is the number of microtubules guided at the boundary wall, N_{total} is the total number of microtubules approaching the boundary wall (guided microtubules and microtubules leaving the structure at the wall).

Following the method used by Clemmens et al[76], the standard error (S_E) for the guiding efficiency was calculated as:

$$S_E = \sqrt{\frac{E\,(1-E)}{N_{total}}} \tag{4.2}$$

Guiding efficiency was examined for gliding motility assay on rectangular nanostructures. The following conditions were evaluated:

1. Attachment of kinesin motors on the surface by non-specific (adsorption on casein) and specific (immobilization with antibodies) means

2. Kinesin-1 protein expressed in different systems (bacterial cells versus insect cells)

3. *In vitro* microtubule polymerization and stabilization methods

Kinesin motors non-specifically adsorbed on casein coated surface efficiently guides the gliding microtubules in nanostructures

For these experiments, recombinant (expressed in *E.coli*) kinesin consisting of full length *D. melanogaster* kinesin-1 heavy chain, flanked with a C-terminal histidine-tag was used[23].

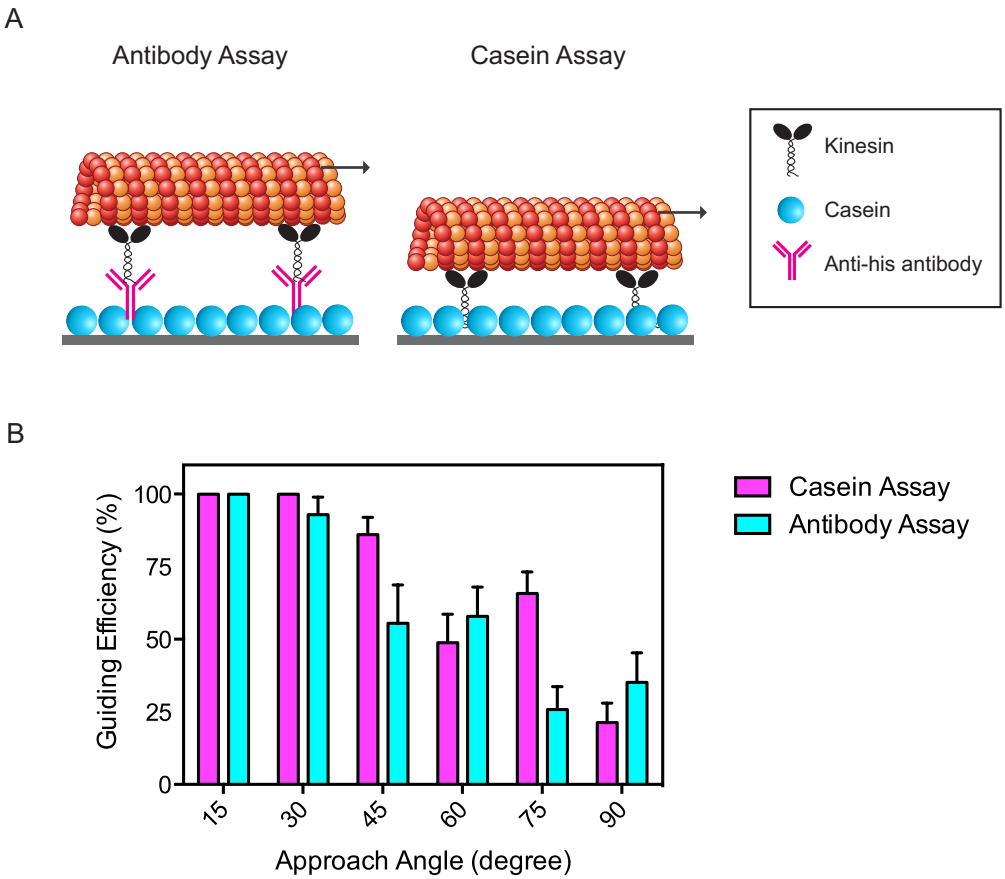

Figure 4.2: Guiding efficiency in casein assay and antibody assay. - A. Schematic showing the setups for the antibody gliding motility assay (Antibody Assay, left) and the casein gliding motility assay (Casein Assay, right). B. Angle dependence of guiding efficiency for the two assay setups (mean ± standard error). The magenta bars represent the guiding efficiencies for the casein assay, while the cyan bars represent that for the antibody assay.

In a gliding motility assay, the kinesin proteins can be immobilized on the

surface either through non-specific surface absorption on a layer of casein (Casein assay), or through specific attachment to surface immobilized anti-his antibodies (Antibody assay). The assay schemes are shown in Figure 4.2A. The efficiency of guiding microtubules in the nanostructures was compared between the casein assay and the antibody assay setups.

Figure 4.2B shows the angle dependence of guiding efficiency of microtubules approaching a boundary wall for the casein assay (magenta) and antibody assay (cyan). A decrease in guiding efficiency with increasing approach angle of microtubule at the boundary wall was observed for both the assay setups. For small approach angles (upto 30°), the guiding efficiency was 100% in both the assays, implying that all microtubules approaching the boundary wall at these angles continued to follow the wall and be guided within the channels. At higher approach angle, the casein assay achieved relatively better microtubule guiding efficiency compared to the antibody assay. The overall average guiding efficiencies were 70.3 ± 5.0 % and 61.2 ± 7.9 % for the casein assay and antibody assay respectively. The casein gliding motility assay with bacterial expressed kinesin thus exhibited relatively improved performance compared to the antibody gliding assay on the nanostructures.

Kinesin motors expressed in insect cells improves guiding efficiency in nanostructures

Traditionally, the kinesin motors used for nanotechnological applications are purified *in vitro* using a bacterial expression system[23]. Recently, an insect cell expression system for his-tagged kinesin construct from *D. melanogaster* was developed in the lab. As the insect cell expression provides more conducive environment (eukaryotic chaperons and post-translational machinery) for the protein, the insect-cell expressed kinesin was found to show higher purity and improved activity compared to the same protein sequence expressed in bacteria[125]. Here, the guiding efficiency of gliding microtubules in nanofabricated structures was evaluated with the kinesin purified from the two expression systems - bacterial expression system and insect expression system. A casein gliding motility assay

setup (that demonstrated better gliding than the antibody assy setup, see 4.1) was used for to compare the effect of the two kinesins.

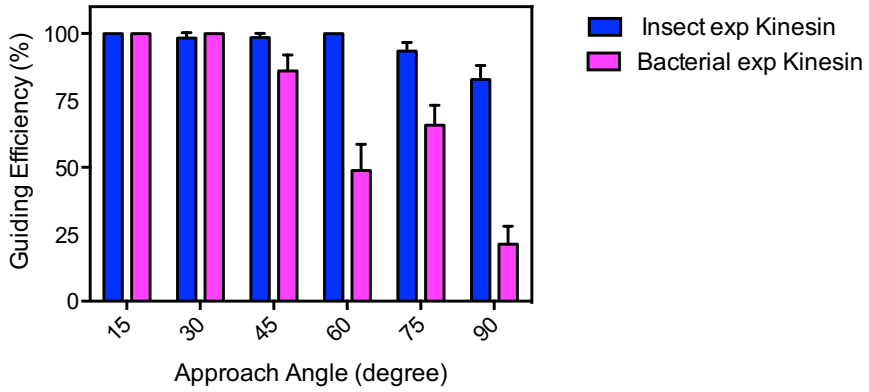

Figure 4.3: Guiding efficiency for casein gliding motility assay with insect-cell expressed kinesin and bacterial expressed kinesin. - Angle dependence of guiding efficiency for the casein gliding motility assay set-up with two different kinesins (mean ± standard error). The blue bars represent the insect-cell expressed kinesin, while the magenta bar corresponds to the bacteria-expressed kinesin

Figure 4.3 shows the angle dependence of guiding efficiency of microtubules approaching a boundary wall for the kinesin expressed in insect cells (blue) and kinesin expressed in bacterial cells (magenta). For both the kinesin expressions, microtubules were successfully guided for when they approached the boundary wall at angles below 30°. For kinesin expressed in bacteria, the guiding efficiency dropped to almost 50 % at approach angles higher than 45°. On the other hand, for kinesin expressed in insect cells, high guiding efficiencies (close to 100 %) was observed for approach angles as high as 75°. Even at higher angles (75–90°), the guiding efficiency was observed to be around 83 %. The overall average guiding efficiencies were 70.3 ± 4.9 % and 95.5 ± 1.2 % for kinesin expressed in bacteria and kinesin expressed in insect cells, respectively. Except for very specific design geometries[75,78], the remarkably high guiding efficiency observed for insect-cell expressed kinesin is higher than almost all of the previously reported microtubule guiding efficiencies[72,77,123]. This demonstrates that kinesin expressed in eukaryotic

expression system of insect cell exhibit superior performance compared to kinesin expressed in prokaryotic bacterial expression system.

Lower flexural rigidity of microtubules improves guiding efficiency in nanostructures

Microtubules are the stiffest intracellular cytoskeletal filaments[126]. Several studies have shown that the stiffness of the microtubules can be tuned by varying the nucleotide used to polymerize microtubule and by changing the stabilizing agent used to prevent depolymerization of the microtubules[59,127–129]. The most common method of preparing microtubules *in vitro* involves polymerizing tubulin with GTP, followed by stabilization with taxol. Microtubules prepared by this method has been shown to have flexural rigidity of $2.5 \pm 0.5 \times 10^{24}$ Nm^2[129]. Alternatively, microtubules can be polymerized using the slowly hydrolyzable nucleotide analogue – GMPCPP. This results in stiffer microtubules, with flexural rigidity of $8 \pm 2 \times 10^{24}$ Nm^2[129]. A third method of preparing microtubule that greatly enhances their long-term stability of the microtubules involves microtubule polymerization with GMPCPP, followed by stabilization with taxol. These "double-stabilized" microtubules have a flexural rigidity of $8 \pm 3 \times 10^{24}$ Nm^2[129], similar to that of the GMPCPP polymerized microtubules.

While long-term stability of microtubules is desirable for several nanotechnological applications, it is important to gain a wholesome understanding of how the stiffness of the microtubules affect the performance of gliding microtubules in nanostructured devices. To investigate that, guiding efficiency of gliding microtubules was evaluated for the three methods of microtubule preparation, in a casein gliding motility assay with insect-cell expressed kinesin motors.

Figure 4.4 shows the angle dependence of guiding efficiency of microtubules approaching a boundary wall for the following microtubule preparations: GTP polymerized microtubules stabilized with Taxol (GTP-Taxol, blue), GMP-CPP polymerized microtubules (CPP, magenta), and GMP-CPP polymerized microtubules stabilized with Taxol (CPP-Taxol, cyan). The flexible GTP-Taxol microtubules were found to have an almost 100 % guiding efficiency upto a high approach angle of 60°. Even at higher approach angles (75-90°), the GTP-Taxol

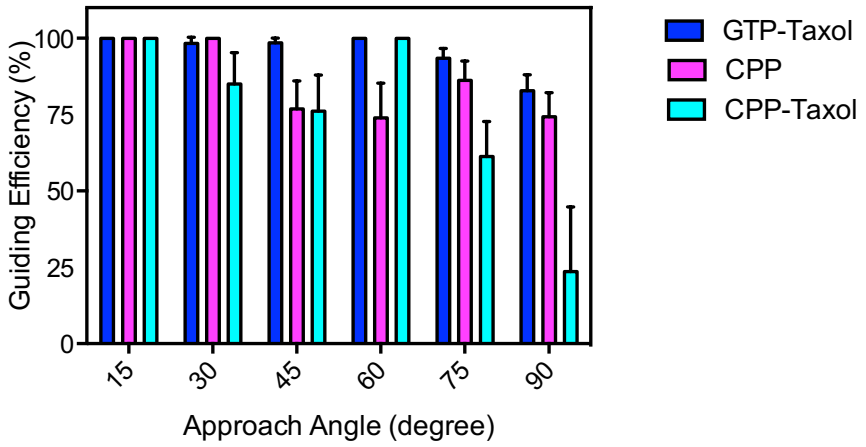

Figure 4.4: Guiding efficiency for various microtubules in a casein gliding motility assay. - Angle dependence of guiding efficiencies (mean ± standard error) for the flexible GTP-Taxol microtubules (dark blue bars), and the stiff GMP-CPP stabilized microtubules (magenta bars) and the GMP-CPP and taxol stabilized microtubules (cyan bars).

microtubules continued to be efficiently guided after encountering a boundary wall. In contrast, the stiffer CPP microtubules and the CPP-Taxol microtubules showed lowered guiding efficiencies at high angles of approach. The performance of the CPP-Taxol microtubules was found to be the worst at higher approach angles (75-90°). The overall guiding efficiencies were found to be 95.5 ± 1.2 %, 85.2 ± 5.8 %, and 74.3 ± 9.1 % for the GTP-Taxol, CPP, and CPP-Taxol microtubules respectively. Thus, the most flexible GTP-Taxol microtubules achieved the highest guiding efficiency on nanostructures in a casein gliding motility assay with insect-cell expressed kinesin.

4.2 Concentrator device

Development of ultrasensitive biosensors is crucial for viable point-of-care diagnostic applications. The concentration of biomarkers in clinical samples often fall in the nM range and lower, necessitating the concentration of samples by centrifugation and other methods before analysis to be in the dynamic detection

range of the employed techniques. These pre-processing steps limits the application of the existing detection methods in a high-throughput, point-of-care setting. While the kinesin-microtubule system has been extensively used to demonstrate proof-of-principle biosensing and analyte detection applications, improvement in detection limit is required for translation of these applications to a practical clinical setting. Here, the nanostructures, that are used to spatially control directionality of the gliding microtubules, are used to achieve analyte concentration as well, by transporting them from a larger loading region to a smaller detection region, to improve detection.

The concentrator device design is shown in Figure 4.5. The flower-shaped design guides the microtubule movement from the wider petal-shaped regions to the circular center, effectively concentrating the microtubules to the center. Analyte bound to the microtubules will also be transported to the center and get concentrated in the process (analyte from a larger region will now be restricted to a smaller region thereby concentrating them), improving the detection limit.

Efficiency of the concentrator device

Different designs of the concentrator device were evaluated for microtubule concentration efficiency. The flower-shaped structures consisted of either 8 or 10 petals, with three different diameters of the central disk (30 μm, 45 μm, 60 μm). The efficiency of each of the design was evaluated with concentration factor that calculates the relative increase in intensity (of the microtubules) at the center.

As the fluorescent microtubules move from the petals to the central circle, there is a corresponding decrease in fluorescence intensity in the petals, and an increase in fluorescence intensity at the center. By manually defining a circle corresponding to the central disk of the device, the observed increase in mean intensity with time was measured (Figure 4.6) to evaluate the concentration factor. For the designs evaluated, the concentration factor was found to increase with time roughly for the first 3 min (imaging started immediately after adding the microtubule solution), but declined thereafter in almost all cases. This happens because in this time frame, the central region of the nanostructures gets saturated with microtubules, and therefore, any additional microtubule trying to get "concentrated" to this

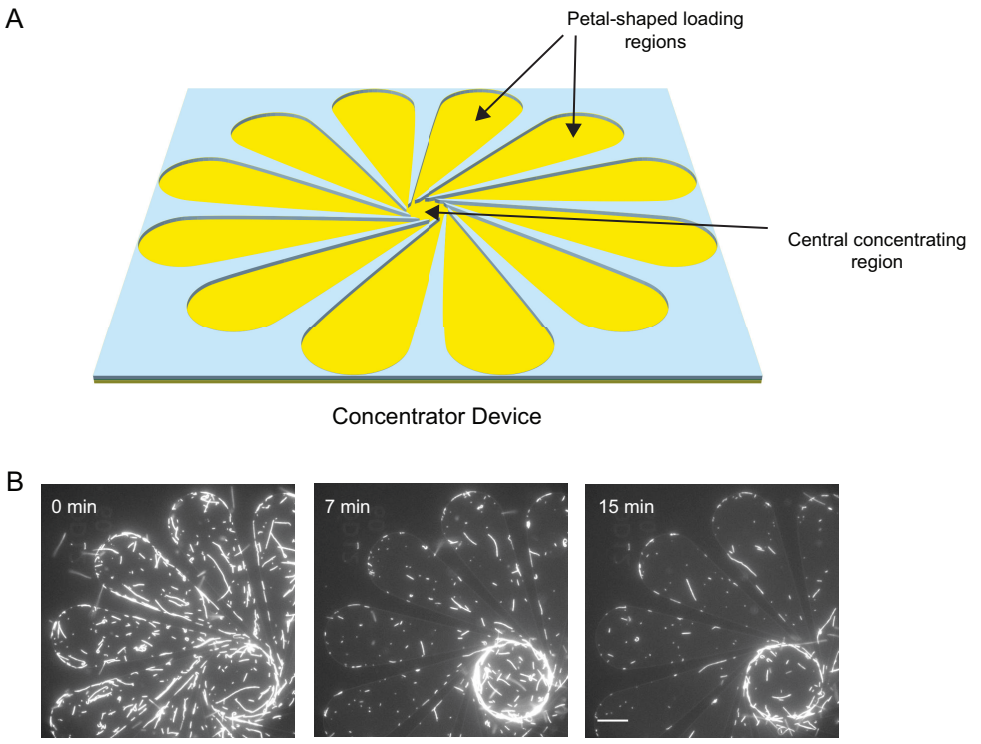

Figure 4.5: Concentrator device. - A. The design of concentrator device. The flower-shaped device consists of multiple petal-shaped loading regions that spatio-temporally concentrate the gliding microtubules to the central concentrating region (Image courtesy: Till Korten). B. Fluorescence images of rhodamine labeled microtubules concentrated to the centre of the concentrator device with time. Scale bar 25 µm

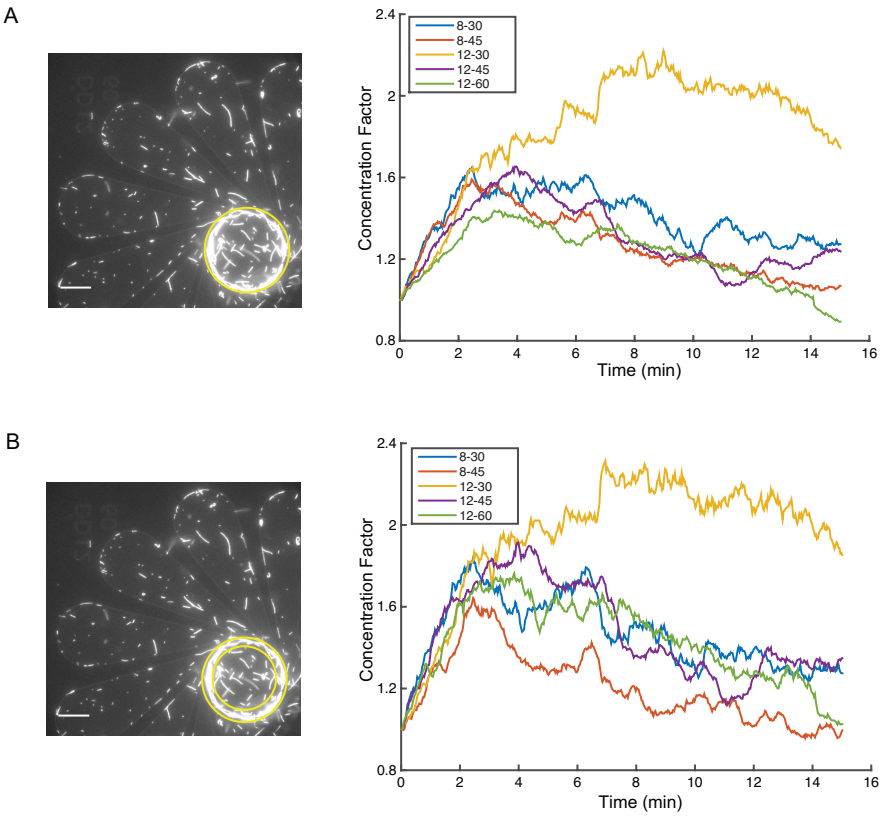

Figure 4.6: Efficiency of the concentrator device. - Concentration efficiency was evaluated for various device design. Each of the identically-processed devices consisted of 8 or 12 petals, with different diameter of the cental circle. The number of petals (P) and the diameter of the circle (C, in μm) are indicated in the graph legend as P-C. A. Fluorescence image of rhodamine labeled microtubules concentrated at the center of the device. The increase in fluorescence intensity with time is followed for the central region (yellow circle demarcating the center) to quantify the concentration factor. B. As the microtubules are concentrated mostly in a ring-shaped region along the periphery of the central region, the increase in fluorescence intensity with time is monitored for this ring-shaped region (yellow circles, left image) to quantify the concentration factor. Scale bar 25 μm

already-microtubule crowded region gets detached from the nanostructure surface, lowering the concentration factor at later times.

Also, it was observed that the concentrated microtubules were restricted only to the periphery of the central region, and were gliding in a ring shaped region along the circumference. Therefore, a second evaluation method was employed, where a ring shaped region was defined as the concentrator region, and instead of observing the intensity change in the whole central disk, intensity change due to concentration of the microtubules was evaluated only for this ring-shaped region (Figure 4.6). The concentration factor was found to be relatively higher in this case, reaching almost twice the initial intensity within the first 3-5 min for most device designs. The decline in the concentration factor was observed after the first 3-5 min, similar to the previous evaluation.

The overall concentration factor (for the first 5 min) ranged from about 1.5 to almost 3. A high variability in the concentration factor was observed, even between identical device designs. The performance of the 12 petal designs was usually better than that of the 8 petal design. However, no clear effect changing the central diameter was observed.

Microvesicle transport and detection in the concentrator device

Next, the concentrator devices were used to concentrate microtubules that capture and transport microvesicles from a cell-line derived sample. Microvesicles are membrane bound sacs shed from almost all cell types, and are important biomarkers for disease diagnosis. Here, purified microvesicles from leukemia cell line were used to demonstrate proof-of-principle application of using microtubule-kinesin system in an on-chip detection system.

Anti-CD45 monoclonal antibody-conjugated microtubules (Ab-MTs) were prepared as described earlier (see Chapter 2). Human T-cell leukemia cell line DND41 and human osteosarcoma cell line MG63 were used to purify leukemic CD45+ and control CD45- microvesicles respectively. The cell lines were labeled with fluorescent dye prior to microvesicle isolation, yielding fluorescent microvesicles.

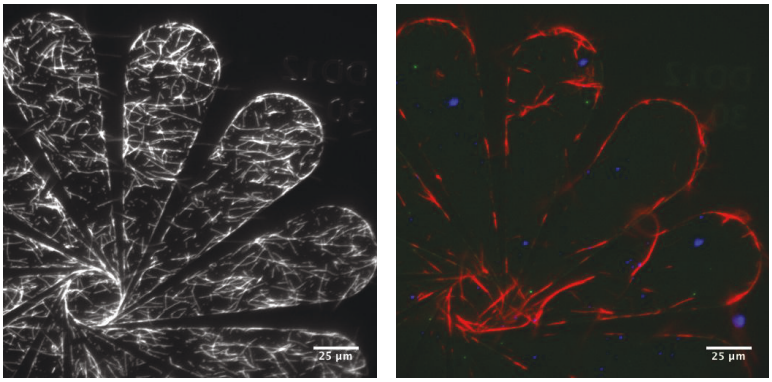

Figure 4.7: Microvesicle transport in the concentrator device. - Fluorescence images of the antibody-conjugated microtubules before (left) and after (right, red microtubules) the addition of the leukemia microvesicles

The fluorescent microvesicles were added in motility solution to the concentrator devices. As observed in Chapter 2, the gliding Ab-MTs can selectively capture and transport the CD45+ leukemia microvesicles. Additionally, the leukemia microvesicles with multiple CD45 sites on their surface cross-linked the gliding Ab-MTs, causing the latter to bundle into larger supramolecular assemblies. Unlike the single microtubule filaments, these large Ab-MT bundles, with their impaired motility and much larger dimensions, could no longer be "guided" by the concentrator device to move to the central disc. As a consequence of this Ab-MT bundling, the application of the concentrator devices towards the development of an on-chip microvesicle detection system proved unsuccessful.

4.3 Conclusion

Lithographically patterned nanostructures have emerged as a promising approach to control directionality of microtubule motility *in vitro*. Here, the effect of fundamental constituents – the assay setup, kinesin motor from different expression systems, microtubule preparation methods – on the efficiency of guiding microtubule motility in the nanostructures was investigated. An optimized assay protocol was established based on the evaluated parameters, with improved motility and robust guidance of gliding microtubules in the nanostructures. These develop-

ments would allow exploration of more challenging nanotechnological applications based on the biomolecular motor system.

Specific design of the nanostructures was then used to develop spatial guidance aided spatio-temporal concentration of microtubules. The concentrator devices achieved almost two-fold increase in microtubule concentration in some designs within a 5 min timeframe. While the concentration factor was not as remarkable as those reported by some earlier designs[9], there is potential to improve the current design to enhance the device performance – for example by capping the central collector region to arrest escaping microtubule following saturation of binding sites, or using a spiral rectifier at the center instead of one uniform circular patch to enable the concentrated microtubule to access the entire region (instead of being restricted in the peripheral ring, in our current example). Nevertheless, with the optimized assay protocol in place, development of next generation concentrator devices with improved performance is feasible.

While the proof-of-principle application of using microtubule transport in concentrator device to detect medically-relevant microvesicles was thwarted by the bundling of microtubules due to the analyte, several examples of highly sensitive analyte detection with antibody-conjugated microtubules on glass surface suggests that the system could be adapted for concentrator devices, particularly for the detection of monovalent analyte. Optimized device design[9,74], enhanced fluorescence detection[130], and magnetic pre-separation of analyte[131] for improved sensitivity are some other strategies in the direction of development of practical diagnostic application with biomolecular motors systems.

5

Summary and outlook

This thesis describes experimental work at the interface of biology, chemistry, and nanotechnology to addresses some of the current challenges in the development of nanotechnological applications using biomolecular motors. Microtubules and kinesin motor proteins were used *in vitro* to reconstitute the highly efficient biomolecular transport. These biological components were then chemically modified to impart functionalities, such as, synthetic cargo transport capability, in order to develop nanotechnological applications.

A robust conjugation scheme to covalently conjugate microtubules was developed using the recently described bioorthogonal, iEDDA reaction between tetrazine and *trans*-cyclooctene. This latest class of "click chemistry" reaction was successfully applied to load a variety of cargo to the microtubules, such as, fluorescent dye, antibodies, and streptavidin.

The effect of flexible PEG linker length on the cargo attachment to microtubules was investigated using the developed conjugation scheme. Increase in the linker length was found to enhance the cargo loading to the microtubules. Moreover, attachment of cargo to microtubules *via* linker longer than the dimension of kinesin motor head was found to rescue the decreased transport velocity reported earlier on loading cargo to microtubules.

The microtubules with covalently conjugated antibodies were used in gliding motility assays to engineer biosensing applications. Highly selective, fluorescence-based detection of protein analyte was achieved using a TIRF microscope setup. Label-free detection of microvesicles and proteins was engineered using the

supramolecular self-assembly of antibody-conjugated-microtubules gliding over the kinesin surface. This label-free detection method was also employed to profile cross-reactivity between commercially available secondary antibodies.

Finally, lithographically patterned nanostructures were used to successfully guide microtubules in a gliding motility assay and achieve spatio-temporal concentration of the gliding microtubules (with/without cargo). The basic assay parameters were optimized to obtain efficient guiding of the gliding microtubules in these nanostructures.

5.1 Outlook

Versatile cargo conjugation The covalent cargo conjugation scheme developed in Chapter 2 is a promising alternative to the non-covalent streptavidin-biotin conjugation traditionally used in the field. The straightforwardness of the protocol developed, coupled with the recent commercial availability of the reagents with different functionalities, makes this scheme promising for the conjugation of a variety of cargo to microtubules *in vitro*. Additionally, the iEDDA chemistry is orthogonal to other "click reactions", opening up possibilities for the simultaneous and/or sequential assembly of multiple modular units to microtubules.

Analyte detection The biosensing applications developed - fluorescence-based as well as the label-free analyte detection schemes - are both based on molecular recognition by antibodies. As antibodies are gold standard affinity probes, the detection methods reported in this thesis are pertinent proof-of-principle applications that can be extended to the detection of a wide range of analytes. A direct future application would entail employing gliding microtubules as a surface for ELISA-type of detection assay. Such an assay, where analyte is detected by antibodies covalently conjugated to gliding microtubules, would retain the advantages of the traditional ELISA assays, while conferring the additional distinction of specifically transported analyte from non-specific stationary molecules that bind to the surface of the assay chamber. The basis for such an assay has already been developed in this thesis, and proof-of-principle applications have been demonstrated with model protein analytes and cell-derived protein samples. Moreover, the example

of abl-bcr fusion protein detection shows that gliding microtubules can also act as a substrate to pull-down specific biomolecules with affinity for α or β tubulin, or detect the presence of microtubule-associated proteins (MAPs) from a sample. As microtubule-kinesin transport has been shown to be compatible to a wide variety of sample solutions[101], further development of novel detection assays for point-of-care diagnosis will be a promising area to explore.

Motor-roadblock studies *In vivo*, the motor proteins transport their cargo along the microtubules while successfully navigating through the highly crowded cellular environment. As breakdown of this transport machinery is related to several pathological conditions, it is crucial to understand how the motor proteins circumvent obstacles encountered during transport. *In vitro*, the purified motor proteins function optimally in different buffer systems, making it challenging to compare the behaviour of different motor proteins to factors such as the amount of roadblocks present on the microtubule surface. The covalent conjugation of roadblocks to microtubules, developed in Chapter 2, overcomes this challenge by providing a setting to compare how different motor proteins navigate obstacles *in vitro*. Characterization of different motor proteins (in their respective buffer systems) stepping on microtubules with covalently conjugated permanent roadblocks will help us understand how different motor proteins navigate around obstacles and what are the different strategies employed to do so.

Assay on nanostructures To generate controlled motion of gliding microtubules, spatial rectification of microtubule motion in lithographically patterned nanostructures have been most successful till date. An important gap in the practical translation of these chip-based assays was addressed in this thesis by investigating how the basic components of the assay influence the microtubule guiding efficiency in the chips. This led to the establishment of optimized parameters for achieving successful control of microtubule motility in nanotechnological applications. Finally, further work can integrate the bioconjugation scheme and the detection principles of the biosensing assays for controlled motility on the nanostructures towards the development of real-world point-of-care diagnostics applications.

6

Materials and methods

6.1 Reagents

Anti-Abl antibody Antibodies-online, Catalog no.: ABIN885839

Anti-Bcr antibody, AlexaFluor488 Antibodies-online, Catalog no.: ABIN879125

Anti-goat antibody Thermo Fisher Scientific, Catalog no.: A-21081

Anti-hAbl antibody R & D Systems, Catalog no.: AF5414

Anti-hBcr antibody R & D Systems, Catalog no.: AF5129

Anti-hCD45 antibody R & D Systems, Catalog no.: MAB1430

Anti-mouse antibody, Alexa Fluor 488 conjugate Thermo Fisher Scientific, Catalog no.: A-11001

ATP Roche Diagnostics GmbH, Catalog no.: 1051998700

Catalase Sigma, Catalog no.: C40

CellTracker™ Deep Red Dye Thermo Fisher Scientific, Catalog no.: C34565

CellTracker™ Green CMFDA Dye Thermo Fisher Scientific, Catalog no.: C7025

Coverslips Menzel Gläser

DMSO Sigma, Catalog no.: 276855

DTT Fermentas, Catalog no.: R0862

EDTA VWR, Catalog no.: 443885J

EGTA Sigma, Catalog no.: E4378

Glucose Oxidase SERVA, Catalog no.: 22778

GMPCPP Jena Bioscience, Catalog no.: NU-405L

GTP Roche Diagnostics GmbH, Catalog no.: 10106399

KOH Merck, Catalog no.: 1.05012.1000

Methanol VWR, Catalog no.: 1.06009.2500

Methyl-Tetrazine-ATTO-488 Jena Bioscience, Catalog no.: CLK-021-02

Methyl-Tetrazine-PEG5-NHS Jena Bioscience, Catalog no.: CLK-A138-10

Parafilm Bemis Company

PIPES Sigma Aldrich, Catalog no.: 80635-250g

Streptavidin, AlexaFluor488 Thermo Fisher Scientific, Catalog no.: S11223

Streptavidin, AlexaFluor546 Thermo Fisher Scientific, Catalog no.: S11225

Taxol Sigma, Catalog no.: T7191

TCO-NHS Jena Bioscience, Catalog no.: CLK-1016-25

TCO-PEG4-NHS Jena Bioscience, Catalog no.: CLK-A137-10

TCO-PEG12-NHS Iris Biotech, Catalog no.: TCO1020.0010

6.2 Buffers

BRB80 80 mM PIPES/KOH, pH 6.9; 1 mM EGTA, 1 mM $MgCl_2$.

BRB80T 10 µM taxol containing BRB80 solution.

High pH cushion: 0.1 M HEPES/NaOH, pH 8.6, 1 mM $MgCl_2$, 1 mM EGTA, 60 % (v/v) glycerol.

Labeling buffer: 0.1 M HEPES/NaOH, pH 8.6, 1 mM $MgCl_2$, 1 mM EGTA, 40 % (v/v) glycerol.

Stop solution: 2x BRB80 with 100 mM K-Glutamate and 40 % (v/v) glycerol.

Low pH cushion BRB80 supplemented with 60 % (v/v) glycerol.

Motility solution 1 mM ATP, 20 mM D-glucose, 20 µg/ml glucose oxidase, 10 µg/ml catalase, 0.5 % β-mercapto-ethanol, 10 µM taxol in BRB80.

Piranha solution 175 ml H_2SO_4 (70 %) + 75 ml H_2O_2 (30 %). Mixed by **slowly** adding H_2O_2 to H_2SO_4. (Note: solution highly corrosive! Handle with care in fume hood only.)

6.3 Kinesin-1 and microtubules

Full length Kinesin-1 was purified using an insect cell expression system by Till Korten and Marcus Braun with help from the Protein Expression facilty at the MPI-CBG (protocol published[125]). Tubulin was purified from pig brain following established protocol[132]. Corina Bräuer conducted the tubulin purification, with help from all the members of the Diez lab.

Functionalization of microtubules

Microtubules were functionalized as described by Hyman et al.[133].

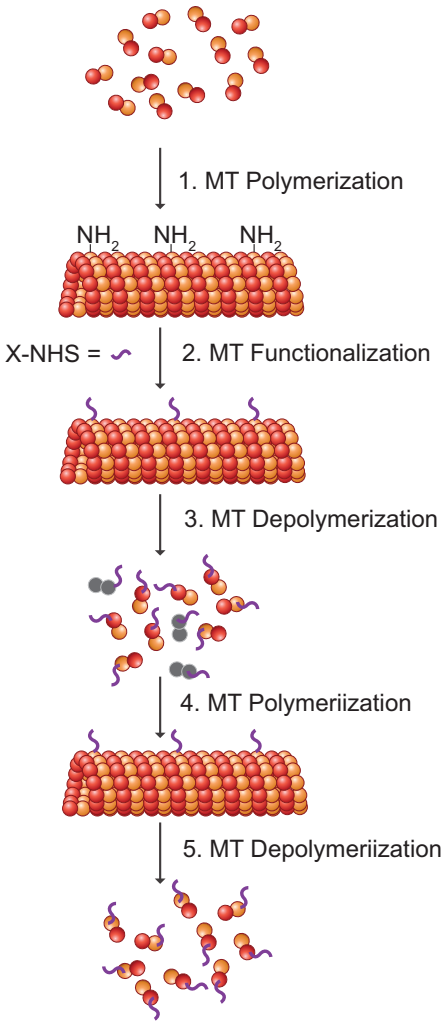

Figure 6.1: Microtubule functionalization. - (1, 2) Polymerized microtubules were functionalized with X-NHS ester reagent. (3, 4) The functionalized microtubules were subjected to a cycle of depolymerization and re-polymerization to separate the functional tubulin from the non-functional tubulin (gray). (5) The microtubules are depolymerized to obtain functionalized tubulin.

Tubulin at high concentration (usually 4.5 ml of 13 mg/ml tubulin) was mixed with 0.5X BRB80, 1 mM GTP, 3.5 mM $MgCl_2$ and 33% glycerol, and incubated on ice for 5 min. Thereafter, microtubules were polymerized by transferring the mixture to a 37 ° C water bath and incubating for 1 h. The polymerized microtubules were spun through a high pH cushion in a pre-warmed MLA80 rotor at 50 000 rpm for 45 min. The pellet obtained was carefully rinsed twice with warm BRB80 at 37 ° C, and then resuspended in 37 ° C warm labeling buffer. The N-Hydroxysuccinimide (NHS)-functionalized reagent was dissolved in dimethyl sulfoxide (DMSO), added to the labeling buffer solution and incubated for 30 min at 37 ° C to label the solvent accessible amino groups on the microtubules. To end the labeling reaction, two reaction volumes of stop solution was added to the mixture and incubated for 5 min. The labeled microtubules were then layered onto a low pH cushion and centrifuged in a pre-warmed MLA80 rotor at 50 000 rpm for 60 min at 37 ° C. The pellet obtained was rinsed thrice with BRB80 solution pre-warmed at 37 ° C and then resuspended in 1 ml

ice cold injection buffer. The solution was transferred to a 2 ml douncer (cooled on ice), and occasionally dounced while incubating on ice for at least 40 min, to obtain a clear homogeneous solution of depolymerized microtubules. These depolymerized microtubules were centrifuged in a precooled MLA130 rotor at 60 000 rpm for 30 min at 4 ° C. The supernatant was recovered and supplemented with 5X BRB80, GTP and $MgCl_2$ to a final concentration of 1X, 1 mM and 4 mM respectively. This mixture was incubated on ice for 3 min, then in a 37 ° C water bath for 2 min. Glycerol was added corresponding to 33% of the final total mixture volume. The solution was then vortexed and incubated at 37 ° C for 30 min to polymerize microtubules from the labeled tubulin. The polymerized microtubules were then layered onto a prewarmed low pH cushion and centrifuged at 50 000 rpm in a pre-warmed MLA80 rotor for 30 min at 37 ° C. The pellet was rinsed twice with warm BRB80 and resuspended in ice cold BRB80. The resuspended pellet solution was incubated on ice for about 30 min to depolymerize the microtubules. The depolymerized microtubules were then centrifuged in a pre-cooled MLA130 rotor at 60000 rpm for 10 min at 4 ° C. The supernatant comprising labeled tubulin was recovered. The concentration of tubulin was estimated by measuring the absorption at 280 nm (extinction coefficient of tubulin dimers is 115000 $M^{-1}cm^{-1}$). The labeled tubulin was then aliquoted at 4 mg/ml and stored at -80 ° C (or liquid nitrogen for long-term storage).

Preparation of microtubules

Microtubules were prepared using the following three methods:

Taxol-stabilized microtubules (Tx-MTs) To prepare Tx-MTs, a polymerization pre-mix solution was prepared with 1.8 µl BRB80, 1.2 µl DMSO, 1 µl 100 mM $MgCl_2$, 1 µl 25 mM GTP. 1.25 µl of this solution was added to 5 µl of 4 mg/ml tubulin and incubated at 37 ° C. After 30-60 min, the polymerized microtubules were stabilized and diluted 100-fold in BRB80T solution.

GMP-CPP stabilized microtubules (CPP-MTs) To prepare CPP-MTs, 64 µl BRB80, 1 µl 100 mM $MgCl_2$ and 10 µl 10 mM GMPCPP were added to

5 µl of 4 mg/ml tubulin solution and incubated at 37 ° C overnight. Thereafter, the BRB80 was added and the microtubule solution centrifuged at 17 000 g in an airfuge for 5 min. The supernatant was discarded and the pellet was resuspended in BRB80.

Double-stabilized microtubules (dsMTs) To prepare ds-MTs, 64 µl BRB80, 1 µl 100 mM $MgCl_2$ and 10 µl 10 mM GMPCPP were added to 5 µl of 4 mg/ml tubulin solution and incubated at 37 ° C. After 90-120 min, 120 µl of BRB80T was added and the microtubule solution centrifuged at 17 000 g in an airfuge for 5 min. The supernatant was discarded and the pellet was resuspended in BRB80T.

6.4 Cell culture and microvesicle (MV) purification

Human T cell leukemic cell line DND41 and human osteosarcoma cell line MG63 were cultured in RPMI 1640 media and DMEM media respectively (media purchased from GIBCO and supplemented with 10% fetal bovine serum, 2 mM L-Glutamine, 100 U/ml penicillin and 10 U/ml streptomycin), and incubated at 37 ° C and 5% CO2. To isolate MVs, 50 ml of the culture medium from 1000 cells/µl was centrifuged at 250 g for 5 min. The supernatent was taken out and centrifuged at 2500 g for 15 min at 4°C. The cell-free supernatent obtained from this step was centrifuged at 18000 g for 2 hours at 4°C to obtain the MVs. The pellet obtained was resuspended in PBS. To obtain fluorescently-labeled MVs, the DND41 and MG63 cell lines were stained with CellTracker™ Green CMFDA Dye and CellTracker™ Deep Red Dye respectively. 5 µM of the dye was added to the cells in PBS, incubated at 37°C and 5% CO2 for 30 min, followed by removal of the dye-containing PBS media, and resuspension of the cells in their respective culture media. These fluorescently-labeled cells shed fluorescent MVs, which were similarly isolated.

6.5 Fabrication of the nanostructures

A combination of nanofabrication process and chemical adsorption, similar to the one described earlier[123], was used to design the chips. The chips were designed and fabricated through collaboration between Till Korten and members of the Bartha group at TU Dresden.

Briefly, the fabrication process involved sputter deposition of a 100 nm Au layer on a 105 mm silicon (Si) wafer, with two 10 nm-thick Ti adhesion systems sandwiched in between. This was followed by deposition of a 500 nm-thick quartz layer and a resist layer. The resist was developed (with a specific design of mask) after exposure in an optical lithography system. Thereafter, the quartz layer was dry-etched down to the Au layer to complete the nanofabrication process. The chips thus obtained were cleaned in acetone, followed by rinsing with ethanol and nanopure water. To block motility on the channel sidewalls, a protein-repellant coating of poly-ethylene glycol (PEG) self-assembled monolayer (SAM) was then undertaken.

6.6 Assay setup

Preparation and cleaning of cover slips and chips

The glass coverslips were prepared by Corina Bräuer or Valeria Candia Campano.

Easy cleaning of glass coverslips The glass coverslips were placed in teflon holder and soaked in glass container comprising 1:20 dilution of Mucasol. The solution was sonicated for 15 min followed by rinsing the coverslips with a stream of deionized water for 2 min. The glass container with the coverslips was then filled with ethanol. After sonicating for 15 min, the coverslips were rinsed with nanopure water (Milli-Q, Millipore Cooperation, USA), the teflon rack with the coverslips taken out and carefully blown dry with N_2.

Piranha cleaning of glass coverslips and Si chips Samples were put in teflon holder and put in beaker and sonicated for 5 min in ethanol:water (1:1) solution. Thereafter, the samples were rinsed in a stream of deionized water for

2 min. The samples were then soaked in piranha solution kept on hot plate at 60°C for 30-40 min for the glass samples, and 30 s for the Si chips. The samples were then rinsed thrice with nanopure water, taken out from the teflon racks and carefully blown dry with N_2.

PEGylation of glass coverslips and Si chips 50 ml of toluene was measured out in a beaker and 115 mg of PEG-silane added. After stirring the solution to ensure proper mixing of the silane, 40 µl of concentrated HCl was added. The cleaned glass coverslips or the Si chips were placed in a teflon holder and placed in this solution for 18 hours with stirring (with the beaker covered). Thereafter the samples are cleaned by rinsing in toluene (once), ethanol (twice), and nanopure water (twice). The teflon rack with the samples taken out and carefully blown dry with N_2.

Assembly of flow cells

Flow cells were assembled from two cover slips (Corning, 22x22 mm^2 and 18x18 mm^2) by placing thin parafilm stripes parallely in between. The channels thus formed were sealed laterally by melting the parafilm by heating the glass cover slips to approximately 60 - 70°C.

The larger glass coverslips were cleaned by easy-clean procedure while the upper smaller glass coverslip used were PEGylated glass cover slips. For the experiments with the chips, flow cells were assembled by sandwiching the structured Si chip with a PEGylated glass cover slip with stretched parafilm in between.

Gliding assays

Gliding motility assays were performed in the assembled flow cells using standard protocol[93]. A 0.5 mg/ml solution of casein in BRB80 was flowed in and incubated for 2 min. Kinesin-1 solution (12.5 nM) was then added and incubated for 2 min. Finally, a motility solution (1 mM ATP, 20 mM D-glucose, 20 mM glucose oxidase, 10 mM catalase, 10 mM DTT, and 10 µM taxol in BRB80) with the microtubules was added. Excess unbound microtubules were removed by flushing motility solution without the microtubules.

6.7 Image acquisition and data analysis

Gliding assay on glass surface

Fluorescence images were acquired with a Nikon Eclipse Ti microscope (with Perfect Focus System) and a PlanApo 100x (NA 1.49) oil immersion objective lens. For epi-fluorescence imaging, a metal arc lamp (Intensilight, Nikon) was used for excitation along with the appropriate filter sets for rhodamine dye (ex:555/25.Dichroic 561 LP, em: 609/54), Cy5 (ex: 642/20, Dichroic 647 LP, em: 700/75), and Alexa Fluor 488 dye (ex: 475/35, Dichroic 491 LP, em: 525/45). Timelapse images were recorded with a 100 ms exposure time using an electron-multiplying charge-coupled device camera (Andor iXon ultra EMCCD, DU-897U) with NIS-Elements imaging software.

Gliding assays on Si chips

Fluorescence images were acquired using a Zeiss Axiovert 200M inverted optical microscope with a Plan-Apochromat 40x (NA 0.95) air objective. For epi-fluorescence imaging, a metal arc lamp was used for excitation along with the appropriate filter sets for rhodamine dye (ex:535/50, Dichroic 565 LP, em: 610/75), Cy5 (ex: 640/20. Dichroic 660 LP, em: 680/30), and Alexa Fluor 488 dye (ex: 480/40, Dichroic 505 LP, em: 535/50). Timelapse images were recorded with a 100 ms exposure time using an electron-multiplying charge-coupled device camera (Andor iXon ultra EMCCD, DU-897U) with Metamorph imaging software.

Data analysis

All the results presented are from experiments repeated at least three times (except data for section 4.2).

Data analysis was performed using Fiji, MATLAB, FIESTA[134], and GraphPad Prism softwares. Microtubule gliding velocity was evaluated using FIESTA - an in-house MATLAB-based tracking software. The amount of fluorescent cargo (dye, antibodies) on the microtubules was quantified as follows: The integrated intensity in the corresponding fluorescent channel was measured using the microtubules

as the mask. The same mask was used to read out the background from an adjacent empty area, which was then subtracted from the original signal to obtain background-subtracted fluorescence intensities. In Chapter 4, the approach angle of the microtubules was measured by hand in Fiji.

References

[1] H. Hess, J. Clemmens, J. Howard, and V. Vogel. 2002. Surface Imaging by Self-Propelled Nanoscale Probes. *Nano Letters*, 2(2):113–116. 1, 5, 7, 13

[2] S. Diez, C. Reuther, C. Dinu, R. Seidel, M. Mertig, W. Pompe, and J. Howard. 2003. Stretching and Transporting DNA Molecules Using Motor Proteins. *Nano Letters*, 3(9): 1251–1254. 7, 13

[3] L. Jia, S. G. Moorjani, T. N. Jackson, and W. O. Hancock. 2004. Microscale transport and sorting by kinesin molecular motors. *Biomedical microdevices*, 6(1):67–74. 9, 41

[4] M. Platt, G. Muthukrishnan, O. H. William, , and M. E. Williams. 2005. Millimeter scale alignment of magnetic nanoparticle functionalized microtubules in magnetic fields. *Journal of the American Chemical Society*, 127(45):15686–7. 7, 13

[5] S. Ramachandran, K.-H. Ernst, G. Bachand, V. Vogel, and H. Hess. 2006. Selective Loading of Kinesin-Powered Molecular Shuttles with Protein Cargo and its Application to Biosensing. *Small*, 2(3):330–334. 7, 13

[6] G. Bachand, S. Rivera, A. Carroll-Portillo, H. Hess, and M. Bachand. 2006. Active Capture and Transport of Virus Particles Using a Biomolecular Motor-Driven, Nanoscale Antibody Sandwich Assay. *Small*, 2(3):381–385. 7, 8, 16, 41

[7] C. Brunner, C. Wahnes, and V. Vogel. 2007. Cargo pick-up from engineered loading stations by kinesin driven molecular shuttles. *Lab on a Chip*, 7(10):1263. 6, 7, 13, 41

[8] B. Hutchins, M. Platt, W. Hancock, and M. E. Williams. 2007. Directing transport of CoFe2O4-functionalized microtubules with magnetic fields. *Small*, 3(1):126–31. 9

[9] C.-T. Lin, M.-t. Kao, K. Kurabayashi, and E. Meyhofer. 2008. Self-contained, biomolecular motor-driven protein sorting and concentrating in an ultrasensitive microfluidic chip. *Nano letters*, 8(4):1041–6. 6, 9, 41, 51, 65

[10] T. Fischer, A. Agarwal, and H. Hess. 2009. A smart dust biosensor powered by kinesin motors. *Nature Nanotechnology*, 4(3):162–166. 41

REFERENCES

[11] C. Schmidt and V. Vogel. 2010. Molecular shuttles powered by motor proteins: loading and unloading stations for nanocargo integrated into one device. *Lab on a Chip*, 10(17): 2195–8. 1, 5, 6, 7, 13, 41

[12] R. Vale, T. Reese, and M. Sheetz. 1985. Identification of a novel force-generating protein, kinesin, involved in microtubule-based motility. *Cell*, 42(1):39–50. 2

[13] R. D. Vale. 2003. The Molecular Motor Toolbox for Intracellular Transport. *Cell*, 112(4): 467–480. 2

[14] M. P. Sheetz. 1996. Microtubule Motor Complexes Moving Membranous Organelles. *Cell Structure and Function*, 21(5):369–373. 2

[15] N. Hirokawa. 1998. Kinesin and Dynein Superfamily Proteins and the Mechanism of Organelle Transport. *Science*, 279(5350).

[16] N. Hirokawa, Y. Noda, and Y. Okada. 1998. Kinesin and dynein superfamily proteins in organelle transport and cell division. *Current Opinion in Cell Biology*, 10(1):60–73.

[17] G. C. Rogers, S. L. Rogers, T. A. Schwimmer, S. C. Ems-McClung, C. E. Walczak, R. D. Vale, J. M. Scholey, and D. J. Sharp. 2004. Two mitotic kinesins cooperate to drive sister chromatid separation during anaphase. *Nature*, 427(6972):364–70.

[18] N. Hirokawa, Y. Noda, Y. Tanaka, and S. Niwa. 2009. Kinesin superfamily motor proteins and intracellular transport. *Nature Reviews Molecular Cell Biology*, 10(10):682–696. 2

[19] S. A. Kuznetsov, E. A. Vaisberg, N. A. Shanina, N. N. Magretova, V. Y. Chernyak, and V. I. Gelfand. 1988. The quaternary structure of bovine brain kinesin. *The EMBO journal*, 7(2):353–6. 2

[20] G. S. Bloom, M. C. Wagner, K. K. Pfister, and S. T. Brady. 1988. Native structure and physical properties of bovine brain kinesin and identification of the ATP-binding subunit polypeptide. *Biochemistry*, 27(9):3409–16.

[21] R. D. Vale and D. S. Friedman. 1999. Single-molecule analysis of kinesin motility reveals regulation by the cargo-binding tail domain. *Nature Cell Biology*, 1(5):293–297. 2

[22] F. J. Kull, E. P. Sablin, R. Lau, R. J. Fletterick, and R. D. Vale. 1996. Crystal structure of the kinesin motor domain reveals a structural similarity to myosin. *Nature*, 380(6574): 550–5. 3

[23] D. L. Coy, M. Wagenbach, and J. Howard. 1999. Kinesin takes one 8-nm step for each ATP that it hydrolyzes. *The Journal of Biological Chemistry*, 274(6):3667–71. 3, 55, 56

[24] A. Yildiz, M. Tomishige, R. D. Vale, and P. R. Selvin. 2004. Kinesin Walks Hand-Over-Hand. *Science*, 303(5658). 3

[25] A. Yildiz and P. Selvin. 2005. Kinesin: walking, crawling or sliding along? *Trends in Cell Biology*, 15(2):112–120. 3

[26] S. Ray, E. Meyhöfer, R. A. Milligan, and J. Howard. 1993. Kinesin follows the microtubule's protofilament axis. *The Journal of Cell Biology*, 121(5). 3, 4

[27] M. J. Schnitzer and S. M. Block. 1997. Kinesin hydrolyses one ATP per 8-nm step. *Nature*, 388(6640):386–390. 3

[28] E. Meyhöfer and J. Howard. 1995. The force generated by a single kinesin molecule against an elastic load. *Proceedings of the National Academy of Sciences of the United States of America*, 92(2):574–8. 3

[29] R. G. Burns. 1991. alpha, beta, and gamma-tubulins: Sequence comparisons and structural constraints. *Cell Motility and the Cytoskeleton*, 20(3):181–189. 3

[30] J. A. Snyder and J. R. McIntosh. 1976. Biochemistry and Physiology of Microtubules. *Annual Review of Biochemistry*, 45(1):699–720. 4

[31] A. Desai and T. J. Mitchison. 1997. Microtubule polymerization dynamics. *Annual Review of Cell and Developmental Biology*, 13(1):83–117. 4

[32] F. Kozielski, I. Arnal, and R. H. Wade. 1998. A model of the microtubule–kinesin complex based on electron cryomicroscopy and X-ray crystallography. *Current Biology*, 8 (4):191–198. 4

[33] T. Mitchison and M. Kirschner. 1984. Dynamic instability of microtubule growth. *Nature*, 312(5991):237–42. 4

[34] D. N. Drechsel and M. W. Kirschner. 1994. The minimum GTP cap required to stabilize microtubules. *Current Biology*, 4(12):1053–1061. 4

[35] M. Caplow and J. Shanks. 1996. Evidence that a single monolayer tubulin-GTP cap is both necessary and sufficient to stabilize microtubules. *Molecular Biology of the Cell*, 7 (4):663–75. 4

[36] S. Inoué and E. D. Salmon. 1995. Force generation by microtubule assembly/disassembly in mitosis and related movements. *Molecular Biology of the Cell*, 6(12):1619–40. 5

[37] P. B. Schiff and S. B. Horwitz. 1980. Taxol stabilizes microtubules in mouse fibroblast cells. *Proceedings of the National Academy of Sciences of the United States of America*, 77(3):1561–5. 5

[38] L. A. Amos and J. Löwe. 1999. How Taxol® stabilises microtubule structure. *Chemistry & Biology*, 6(3):R65–R69. 5

[39] A. A. Hyman, S. Salser, D. N. Drechsel, N. Unwin, and T. J. Mitchison. 1992. Role of GTP hydrolysis in microtubule dynamics: information from a slowly hydrolyzable analogue, GMPCPP. *Molecular Biology of the Cell*, 3(10):1155–67. 5

[40] D. Turner, C. Chang, K. Fang, P. Cuomo, and D. Murphy. 1996. Kinesin Movement on Glutaraldehyde-Fixed Microtubules. *Analytical Biochemistry*, 242(1):20–25. 5, 6

[41] S. M. Block, L. S. Goldstein, and B. J. Schnapp. 1990. Bead movement by single kinesin molecules studied with optical tweezers. *Nature*, 348(6299):348–52. 6

[42] C. Bottier, J. Fattaccioli, M. C. Tarhan, R. Yokokawa, F. O. Morin, B. Kim, D. Collard, and H. Fujita. 2009. Active transport of oil droplets along oriented microtubules by kinesin molecular motors. *Lab on a Chip*, 9(12):1694. 6

[43] J. Howard, A. J. Hudspeth, and R. D. Vale. 1989. Movement of microtubules by single kinesin molecules. *Nature*, 342(6246):154–8. 6

[44] J. Kerssemakers, L. Ionov, U. Queitsch, S. Luna, H. Hess, and S. Diez. 2009. 3D Nanometer Tracking of Motile Microtubules on Reflective Surfaces. *Small*, 5(15):1732–1737. 6, 41

[45] T. Korten, A. Månsson, and S. Diez. 2010. Towards the application of cytoskeletal motor proteins in molecular detection and diagnostic devices. *Current Opinion in Biotechnology*, 21(4):477–88. 7, 13, 14, 41

[46] L. Chaiet and F. J. Wolf. 1964. The properties of streptavidin, a biotin-binding protein produced by Streptomycetes. *Archives of Biochemistry and Biophysics*, 106:1–5. 7

[47] P. C. Weber, D. H. Ohlendorf, J. J. Wendoloski, and F. R. Salemme. 1989. Structural origins of high-affinity biotin binding to streptavidin. *Science (New York, N.Y.)*, 243 (4887):85–8. 7

[48] H. Hess, J. Clemmens, C. Brunner, R. Doot, S. Luna, K.-H. Ernst, and V. Vogel. 2005. Molecular self-assembly of "nanowires"and "nanospools" using active transport. *Nano letters*, 5(4):629–33. 7, 41, 45

[49] A. T. Lam, V. VanDelinder, A. M. R. Kabir, H. Hess, G. D. Bachand, and A. Kakugo. 2016. Cytoskeletal motor-driven active self-assembly in in vitro systems. *Soft matter*, 12 (4):988–97. 7, 41, 45

[50] T. Buranda, G. P. Lopez, J. Keij, R. Harris, and L. A. Sklar. 1999. Peptides, antibodies, and FRET on beads in flow cytometry: A model system using fluoresceinated and biotinylated beta-endorphin. *Cytometry*, 37(1):21–31. 7

[51] A. Pierres, D. Touchard, A.-M. Benoliel, and P. Bongrand. 2002. Dissecting streptavidin-biotin interaction with a laminar flow chamber. *Biophysical Journal*, 82(6):3214–23.

[52] R. Merkel, P. Nassoy, A. Leung, K. Ritchie, and E. Evans. 1999. Energy landscapes of receptor–ligand bonds explored with dynamic force spectroscopy. *Nature*, 397(6714):50–53. 7

[53] C. Dinu, J. Opitz, W. Pompe, J. Howard, M. Mertig, and S. Diez. 2006. Parallel Manipulation of Bifunctional DNA Molecules on Structured Surfaces Using Kinesin-Driven Microtubules. *Small*, 2(8-9):1090–1098. 7

[54] S. Hiyama, T. Inoue, T. Shima, Y. Moritani, T. Suda, and K. Sutoh. 2008. Autonomous Loading, Transport, and Unloading of Specified Cargoes by Using DNA Hybridization and Biological Motor-Based Motility. *Small*, 4(4):410–415.

[55] S. Taira, Y.-Z. Du, Y. Hiratsuka, T. Q. Uyeda, N. Yumoto, and M. Kodaka. 2008. Loading and unloading of molecular cargo by DNA-conjugated microtubule. *Biotechnology and Bioengineering*, 99(3):734–739.

[56] S. Hiyama, R. Gojo, T. Shima, S. Takeuchi, and K. Sutoh. 2009. Biomolecular-Motor-Based Nano- or Microscale Particle Translocations on DNA Microarrays. *Nano Letters*, 9 (6):2407–2413. 7

[57] A. Carroll-Portillo, M. Bachand, and G. D. Bachand. 2009. Directed attachment of antibodies to kinesin-powered molecular shuttles. *Biotechnology and Bioengineering*, 104 (6):1182–8. 8

[58] R. E. Kleiner, S.-C. Ti, and T. M. Kapoor. 2013. Site-specific chemistry on the microtubule polymer. *Journal of the American Chemical Society*, 135(34):12520–3. 8

[59] L. M. MacDonald, A. Armson, R. C. A. Thompson, and J. A. Reynoldson. 2003. Characterization of factors favoring the expression of soluble protozoan tubulin proteins in Escherichia coli. *Protein Expression and Purification*, 29(1):117–22. 8, 58

[60] S. M. Früh, D. Steuerwald, U. Simon, and V. Vogel. 2012. Covalent Cargo Loading to Molecular Shuttles via Copper-free "Click Chemistry". *Biomacromolecules*, 13(12): 3908–3911. 8, 16

[61] N. J. Agard, J. A. Prescher, and C. R. Bertozzi. 2005. A Strain-Promoted [3 + 2] Azide−Alkyne Cycloaddition for Covalent Modification of Biomolecules in Living Systems. *Journal of the American Chemical Society*, 127(31):11196–11196. 8

[62] J. M. Baskin, J. A. Prescher, S. T. Laughlin, N. J. Agard, P. V. Chang, I. A. Miller, A. Lo, J. A. Codelli, and C. R. Bertozzi. 2007. Copper-free click chemistry for dynamic in vivo imaging. *Proceedings of the National Academy of Sciences of the United States of America*, 104(43):16793–7. 8

[63] N. K. Devaraj and R. Weissleder. 2011. Biomedical applications of tetrazine cycloadditions. *Accounts of Chemical Research*, 44(9):816–27. 8

[64] J. R. Dennis, J. Howard, and V. Vogel. 1999. Molecular shuttles: directed motion of microtubules along nanoscale kinesin tracks. *Nanotechnology*, 10(3):232–236. 9

[65] C. Reuther, L. Hajdo, R. Tucker, A. A. Kasprzak, and S. Diez. 2006. Biotemplated nanopatterning of planar surfaces with molecular motors. *Nano Letters*, 6(10):2177–83. 9

[66] J. Clemmens, H. Hess, R. Doot, C. M. Matzke, G. D. Bachand, and V. Vogel. 2004. Motor-protein "roundabouts": Microtubules moving on kinesin-coated tracks through engineered networks. *Lab on a Chip*, 4(2):83–86. 9, 52

[67] E. Kim, K.-E. Byun, D. S. Choi, D. J. Lee, D. H. Cho, B. Y. Lee, H. Yang, J. Heo, H.-J. Chung, S. Seo, and S. Hong. 2013. Electrical control of kinesin–microtubule motility using a transparent functionalized-graphene substrate. *Nanotechnology*, 24(19):195102. 9

[68] T. Kim, M.-T. Kao, E. F. Hasselbrink, and E. Meyhöfer. 2008. Nanomechanical Model of Microtubule Translocation in the Presence of Electric Fields. *Biophysical Journal*, 94(10): 3880–3892.

[69] M. G. L. van den Heuvel, M. P. de Graaff, and C. Dekker. 2006. Molecular Sorting by Electrical Steering of Microtubules in Kinesin-Coated Channels. *Science*, 312(5775). 9, 52

[70] T. Kim, M.-T. Kao, E. Meyhöfer, and E. F. Hasselbrink. 2007. Biomolecular motor-driven microtubule translocation in the presence of shear flow: analysis of redirection behaviours. *Nanotechnology*, 18(2):025101. 9

[71] R. Stracke, K. J. Böhm, J. Burgold, H.-J. Schacht, and E. Unger. 2000. Physical and technical parameters determining the functioning of a kinesin-based cell-free motor system. *Nanotechnology*, 11(2):52–56. 9

[72] Y. Hiratsuka, T. Tada, K. Oiwa, T. Kanayama, and T. Q. Uyeda. 2001. Controlling the Direction of Kinesin-Driven Microtubule Movements along Microlithographic Tracks. *Biophysical Journal*, 81(3):1555–1561. 9, 51, 57

[73] S. G. Moorjani, L. Jia, T. N. Jackson, W. O. Hancock, and Samira G. 2003. Lithographically Patterned Channels Spatially Segregate Kinesin Motor Activity and Effectively Guide Microtubule Movements. *Nano Letters*, 3(5):633–637.

[74] C.-T. Lin, M.-T. Kao, K. Kurabayashi, and E. Meyhöfer. 2006. Efficient Designs for Powering Microscale Devices with Nanoscale Biomolecular Motors. *Small*, 2(2):281–287. 9, 51, 52, 65

[75] L.-J. Cheng, M.-T. Kao, E. Meyhöfer, and L. Guo. 2005. Highly Efficient Guiding of Microtubule Transport with Imprinted CYTOP Nanotracks. *Small*, 1(4):409–414. 57

[76] J. Clemmens, H. Hess, J. Howard, and V. Vogel. 2003. Analysis of Microtubule Guidance in Open Microfabricated Channels Coated with the Motor Protein Kinesin. *Langmuir*, 19 (5):1738–1744. 54

[77] J. Clemmens, H. Hess, R. Lipscomb, Y. Hanein, K. F. Böhringer, C. M. Matzke, G. D. Bachand, B. C. Bunker, and V. Vogel. 2003. Mechanisms of microtubule guiding on microfabricated kinesin-coated surfaces: Chemical and topographic surface patterns. *Langmuir*, 19(26):10967–10974. 9, 51, 57

[78] H. Hess, C. M. Matzke, R. K. Doot, J. Clemmens, G. D. Bachand, B. C. Bunker, and V. Vogel. 2003. Molecular Shuttles Operating Undercover: A New Photolithographic Approach for the Fabrication of Structured Surfaces Supporting Directed Motility. *Nano Letters*, 3(12):1651–1655. 9, 57

[79] H. Hess and V. Vogel. 2001. Molecular shuttles based on motor proteins: active transport in synthetic environments. *Reviews in Molecular Biotechnology*, 82(1):67–85. 13, 41

[80] M. G. L. van den Heuvel and C. Dekker. 2007. Motor proteins at work for nanotechnology. *Science (New York, N.Y.)*, 317(5836):333–6. 13

[81] J. Howard. 1996. The movement of kinesin along microtubules. *Annual Review of Physiology*, 58:703–29. 13, 41

[82] P. Katira and H. Hess. 2010. Two-Stage Capture Employing Active Transport Enables Sensitive and Fast Biosensors. *Nano Letters*, 10(2):567–572. 13

[83] M. L. Blackman, M. Royzen, and J. M. Fox. 2008. Tetrazine ligation: fast bioconjugation based on inverse-electron-demand Diels-Alder reactivity. *Journal of the American Chemical Society*, 130(41):13518–9. 13

[84] N. K. Devaraj, R. Upadhyay, J. B. Haun, S. A. Hilderbrand, and R. Weissleder. 2009. Fast and sensitive pretargeted labeling of cancer cells through a tetrazine/trans-cyclooctene cycloaddition. *Angewandte Chemie*, 48(38):7013–6. 13

[85] T. Korten and S. Diez. 2008. Setting up roadblocks for kinesin-1: mechanism for the selective speed control of cargo carrying microtubules. *Lab on a Chip*, 8(9):1441. 14, 21

[86] C. Schmidt, B. Kim, H. Grabner, J. Ries, M. Kulomaa, and V. Vogel. 2012. Tuning the "Roadblock" Effect in Kinesin-Based Transport. *Nano Letters*, 12(7):3466–3471. 14, 21

[87] C. M. Soto, B. D. Martin, K. E. Sapsford, A. S. Blum, and B. R. Ratna. 2008. Toward single molecule detection of staphylococcal enterotoxin B: mobile sandwich immunoassay on gliding microtubules. *Analytical Chemistry*, 80(14):5433–40. 16, 41

[88] C. M. Niemeyer. 2004. *Bioconjugation Protocols : Strategies and Methods*. Humana Press. ISBN 9781592598137. 16

[89] P. C. Weber, D. H. Ohlendorf, J. J. Wendoloski, and F. R. Salemme. 1989. Structural origins of high-affinity biotin binding to streptavidin. *Science (New York, N.Y.)*, 243 (4887):85–8. 21

[90] W. A. Hendrickson, A. Pähler, J. L. Smith, Y. Satow, E. A. Merritt, and R. P. Phizackerley. 1989. Crystal structure of core streptavidin determined from multiwavelength anomalous diffraction of synchrotron radiation. *Proceedings of the National Academy of Sciences of the United States of America*, 86(7):2190–4. 21

[91] J. Cooper, J. Shen, F. Young, P. Connolly, J. Barker, and G. Moores. 1940. The imaging of streptavidin and avidin using scanning tunnelling microscopy. *Journal of Materials Science: Materials in Electronics*, 5(2):106–110.

[92] Y. S. Sun, J. P. Landry, Y. Y. Fei, X. D. Zhu, J. T. Luo, X. B. Wang, and K. S. Lam. 2009. Macromolecular scaffolds for immobilizing small molecule microarrays in label-free detection of protein-ligand interactions on solid support. *Analytical Chemistry*, 81(13): 5373–80. 21

[93] B. Nitzsche, V. Bormuth, C. Bräuer, J. Howard, L. Ionov, J. Kerssemakers, T. Korten, C. Leduc, F. Ruhnow, and S. Diez. 2010. Studying kinesin motors by optical 3D-nanometry in gliding motility assays. *Methods in Cell Biology*, 95:247–71. 22, 28, 78

[94] P. Flory and M. Volkenstein. 1969. *Statistical Mechanics of Chain Molecules*. Wiley Online Library. 28

[95] S. Zou, H. Schönherr, and G. J. Vancso. 2005. Stretching and Rupturing Individual Supramolecular Polymer Chains by AFM. *Angewandte Chemie International Edition*, 44 (6):956–959. 28

[96] Https://www.micronics.net. Micronics Inc. 31

[97] Https://www.pointofcare.abbott/int/en/offerings/istat/istat-handheld. Abbott. 31

[98] Http://www.biology-pages.info/C/CML.html. Biology-Pages. 35

[99] J. F. Apperley. 2015. Chronic myeloid leukaemia. *The Lancet*, 385(9976):1447–1459. 35

[100] L. Coulombel, D. K. Kalousek, C. J. Eaves, C. M. Gupta, and A. C. Eaves. 1983. Long-Term Marrow Culture Reveals Chromosomally Normal Hematopoietic Progenitor Cells in Patients with Philadelphia Chromosome-Positive Chronic Myelogenous Leukemia. *New England Journal of Medicine*, 308(25):1493–1498. 35

[101] S. Korten, N. Albet-Torres, F. Paderi, L. ten Siethoff, S. Diez, T. Korten, G. te Kronnie, and A. Månsson. 2013. Sample solution constraints on motor-driven diagnostic nanodevices. *Lab on a Chip*, 13(5):866–76. 39, 69

[102] D. Miroshnychenko, A. Dubrovska, S. Maliuta, G. Telegeev, and P. Aspenström. 2010. Novel role of pleckstrin homology domain of the Bcr-Abl protein: Analysis of protein–protein and protein–lipid interactions. *Experimental Cell Research*, 316(4):530–542. 40

[103] S. X. Leng, J. E. McElhaney, J. D. Walston, D. Xie, N. S. Fedarko, and G. A. Kuchel. 2008. ELISA and Multiplex Technologies for Cytokine Measurement in Inflammation and Aging Research. *The Journals of Gerontology Series A: Biological Sciences and Medical Sciences*, 63(8):879–884. 41

[104] M. X. Rangaka, K. A. Wilkinson, J. R. Glynn, D. Ling, D. Menzies, J. Mwansa-Kambafwile, K. Fielding, R. J. Wilkinson, and M. Pai. 2012. Predictive value of interferon-γ release assays for incident active tuberculosis: a systematic review and meta-analysis. *The Lancet Infectious Diseases*, 12(1):45–55. 41

[105] P. Patel. 2002. (Bio)sensors for measurement of analytes implicated in food safety: a review. *TrAC Trends in Analytical Chemistry*, 21(2):96–115. 41

[106] M. A. Cooper and M. A. Cooper. 2002. Optical biosensors in drug discovery. *Nature Reviews Drug Discovery*, 1(7):515–528. 41

[107] M. A. Cooper. 2003. Label-free screening of bio-molecular interactions. *Analytical and Bioanalytical Chemistry*, 377(5):834–842. 41

[108] S. Ray, G. Mehta, and S. Srivastava. 2010. Label-free detection techniques for protein microarrays: Prospects, merits and challenges. *Proteomics*, 10(4):731–748. 41

[109] M.-J. Banuls, R. Puchades, and A. Maquieira. 2013. Chemical surface modifications for the development of silicon-based label-free integrated optical (IO) biosensors: A review. *Analytica Chimica Acta*, 777:1–16. 41

[110] L. Duan, D. Che, K. Zhang, Q. Ong, S. Guo, and B. Cui. 2015. Optogenetic Control of Molecular Motors and Organelle Distributions in Cells. *Chemistry & Biology*, 22(5): 671–682. 41

[111] H. Hess, J. Clemmens, D. Qin, J. H. And, and V. Vogel. 2001. Light-Controlled Molecular Shuttles Made from Motor Proteins Carrying Cargo on Engineered Surfaces. *Nano Letters*, 1(5):235–239. 41

[112] R. Kawamura, A. Kakugo, Y. Osada, and J. P. Gong. 2010. Microtubule bundle formation driven by ATP: the effect of concentrations of kinesin, streptavidin and microtubules. *Nanotechnology*, 21(14):145603. 41

[113] I. Luria, J. Crenshaw, M. Downs, A. Agarwal, S. B. Seshadri, J. Gonzales, O. Idan, J. Kamcev, P. Katira, S. Pandey, T. Nitta, S. R. Phillpot, and H. Hess. 2011. Microtubule nanospool formation by active self-assembly is not initiated by thermal activation. *Soft Matter*, 7(7):3108–3115.

[114] A. T. Lam, C. Curschellas, D. Krovvidi, and H. Hess. 2014. Controlling self-assembly of microtubule spools via kinesin motor density. *Soft Matter*, 10(43):8731–6.

[115] S. Wada, A. M. R. Kabir, R. Kawamura, M. Ito, D. Inoue, K. Sada, and A. Kakugo. 2015. Controlling the bias of rotational motion of ring-shaped microtubule assembly. *Biomacromolecules*, 16(1):374–8. 41

[116] E. Cocucci, G. Racchetti, and J. Meldolesi. 2009. Shedding microvesicles: artefacts no more. *Trends in Cell Biology*, 19(2):43–51. 42

[117] G. Raposo and W. Stoorvogel. 2013. Extracellular vesicles: exosomes, microvesicles, and friends. *The Journal of Cell Biology*, 200(4):373–83. 42

[118] H. Shao, J. Chung, L. Balaj, A. Charest, D. D. Bigner, B. S. Carter, F. H. Hochberg, X. O. Breakefield, R. Weissleder, and H. Lee. 2012. Protein typing of circulating microvesicles allows real-time monitoring of glioblastoma therapy. *Nature Medicine*, 18(12):1835–40. 43

[119] B. György, M. E. Hung, X. O. Breakefield, and J. N. Leonard. 2015. Therapeutic Applications of Extracellular Vesicles: Clinical Promise and Open Questions. *Annual Review of Pharmacology and Toxicology*, 55(1):439–464.

[120] S. Kumar, G. Milani, H. Takatsuki, T. Lana, M. Persson, C. Frasson, G. te Kronnie, and A. Månsson. 2016. Sensing protein antigen and microvesicle analytes using high-capacity biopolymer nano-carriers. *The Analyst*, 141(3):836–46. 43

[121] E. van der Pol, A. G. Hoekstra, A. Sturk, C. Otto, T. G. van Leeuwen, and R. Nieuwland. 2010. Optical and non-optical methods for detection and characterization of microparticles and exosomes. *Journal of Thrombosis and Haemostasis*, 8(12):2596–2607. 43

[122] M. Baker. 2015. Reproducibility crisis: Blame it on the antibodies. *Nature*, 521(7552): 274–276. 47

[123] M. G. L. van den Heuvel, C. T. Butcher, R. M. M. Smeets, S. Diez, and C. Dekker. 2005. High rectifying efficiencies of microtubule motility on kinesin-coated gold nanostructures. *Nano Letters*, 5(6):1117–22. 51, 52, 53, 57, 77

[124] D. V. Nicolau, M. Lard, T. Korten, F. C. M. J. M. van Delft, M. Persson, E. Bengtsson, A. Månsson, S. Diez, H. Linke, and D. V. Nicolau. 2016. Parallel computation with molecular-motor-propelled agents in nanofabricated networks. *Proceedings of the National Academy of Sciences of the United States of America*, 113(10):2591–6. 51

[125] T. Korten, S. Chaudhuri, E. Tavkin, M. Braun, and S. Diez. 2016. Kinesin-1 Expressed in Insect Cells Improves Microtubule in Vitro Gliding Performance, Long-Term Stability and Guiding Efficiency in Nanostructures. *IEEE Transactions on NanoBioscience*, 15(1): 62–69. 56, 73

[126] T. Hawkins, M. Mirigian, M. Selcuk Yasar, and J. L. Ross. 2010. Mechanics of microtubules. *Journal of Biomechanics*, 43(1):23–30. 58

[127] B. Mickey and J. Howard. 1995. Rigidity of microtubules is increased by stabilizing agents. *The Journal of Cell Biology*, 130(4). 58

[128] H. Felgner, R. Frank, J. Biernat, E. M. Mandelkow, E. Mandelkow, B. Ludin, A. Matus, and M. Schliwa. 1997. Domains of neuronal microtubule-associated proteins and flexural rigidity of microtubules. *The Journal of Cell Biology*, 138(5):1067–75.

[129] T. L. Hawkins, D. Sept, B. Mogessie, A. Straube, and J. L. Ross. 2013. Mechanical properties of doubly stabilized microtubule filaments. *Biophysical Journal*, 104(7):1517–28. 58

[130] D. Axelrod. 2001. Total Internal Reflection Fluorescence Microscopy in Cell Biology. *Traffic*, 2(11):764–774. 65

[131] S. Kumar, L. Ten Siethoff, M. Persson, N. Albet-Torres, and A. Månsson. 2013. Magnetic capture from blood rescues molecular motor function in diagnostic nanodevices. *Journal of Nanobiotechnology*, 11(1):14. 65

[132] M. Castoldi and A. V. Popov. 2003. Purification of brain tubulin through two cycles of polymerization-depolymerization in a high-molarity buffer. *Protein Expression and Purification*, 32(1):83–8. 73

[133] A. Hyman, D. Drechsel, D. Kellogg, S. Salser, K. Sawin, P. Steffen, L. Wordeman, and T. Mitchison. 1991. Preparation of modified tubulins. *Methods in Enzymology*, 196:478–85. 73

[134] F. Ruhnow, D. Zwicker, and S. Diez. 2011. Tracking single particles and elongated filaments with nanometer precision. *Biophysical Journal*, 100(11):2820–8. 79

Publications

1. *Label-free detection of microvesicles and proteins by the bundling of gliding microtubules*
   S. Chaudhuri, T. Korten, S. Korten, G. Milani, T. Lana, G. te Kronnie, and S. Diez.
   Nano Letters (in review).

2. *Tetrazine-trans-cyclooctene-mediated conjugation of antibodies to microtubules facilitates sub-picomolar protein detection*
   S. Chaudhuri, T. Korten, and S. Diez.
   Bioconjugate Chemistry, 28 (4), 918–922 (2017).

3. *Kinesin-1 expressed in insect-cells improves microtubule in vitro gliding performance, long-term stability and guiding efficiency in nanostructures*
   T. Korten, S. Chaudhuri, E. Tavkin, M. Braun, and S. Diez.
   IEEE Transactions on NanoBioscience, 15(1), 62-69 (2016).

Acknowledgements

First and foremost, I would like to thank Prof. Stefan Diez for his brilliance, positivity, and genuineness. Stefan, thank you for welcoming me in your group and guiding me through my PhD. I greatly appreciate the scientific freedom you gave me, and the encouragement and support you provided along the way. Directly and indirectly, I have learned a lot more from you than that can be expressed in an acknowledgement section.

The yearly thesis advisory committee meetings were indispensable in evaluating the scientific progress and readjusting the overall direction of the PhD. I would like to thank Prof. Brigitte Voit and Prof. Yixin Zhang for their time and scientific inputs as my thesis advisory committee members, and for being members of my Doctoral committee as well. I would also like to thank Prof. Voit for her very through and helpful comments on the thesis draft and for reviewing this thesis.

I would like to thank two of my close friends - Dr. Sumeet Pal Singh and Mainak Mustafi - for sharing the excitement to discuss science, for discussing their insights on my projects, and for meticulously editing this thesis.

The concentrator device project that I started my PhD with was initiated by Dr. Till Korten and others long before I joined the lab, which allowed me to draw on the existing resources. Thank you Till, for sharing your expertise, for the good conversations, and for commenting on this thesis.

The friendly and supportive environment in the lab made it a pleasure to go to work. In particular, I would like to thank Dr. Rahul Grover

for patiently replying to all my questions (that started before I joined the lab) and for providing valuable inputs on this thesis; Lara Scharrel and Aniruddha Mitra for getting me started in the lab; and Juliane Beyer for the practical solutions. I will especially miss the lengthy, non-scientific discussions over (mostly boring canteen) food and (Katja's lovely) coffee with you all. I would also like to thank Dr. Cordula Reuther, Dr. Eva Zatecka, Raluca Groza, Alejandra Laguillo Diego, Dr. Marcus Braun, Dr. Zdenek Lansky, Dr. Jens Ehrig , Dr. Annemarie Lüdecke, and Dr. Felix Ruhnow for fruitful discussions, especially during the lab meetings. I would like to thank Corina Bräuer, for ensuring that the lab runs smoothly, and for being so caring.

For taking care of the daunting administrative tasks, I would like to thank Anja Glenk at the International Office and Barbara Lindemann in the Diez lab.

Like most important things in life, these three years in Dresden have been wonderful and difficult at the same time. I am grateful to Nitesh for the unwavering love and support that sustained me through these years and helped me keep perspective. Lastly, but most importantly, I would like to thank my parents for always believing in me and supporting me in every way possible.

Erklärung

Erklärung entsprechend §5.5 der Promotionsordnung

Hiermit versichere ich, dass ich die vorliegende Arbeit ohne unzulässige Hilfe Dritter und ohne Benutzung anderer als der angegebenen Hilfsmittel angefertigt habe; die aus fremden Quellen direkt oder indirekt übernommenen Gedanken sind als solche kenntlich gemacht. Die Arbeit wurde bisher weder im Inland noch im Ausland in gleicher oder ähnlicher Form einer anderen Prüfungsbehörde vorgelegt.

Die Dissertation wurde im Zeitraum vom 25$^{\text{th}}$ August 2014 bis 19$^{\text{th}}$ October 2017 verfasst und von Prof. Dr. Stefan Diez am B CUBE – Center for Molecular Bioengeneering der Technischen Universität Dresden betreut.

Meine Person betreffend erkläre ich hiermit, dass keine früheren erfolglosen Promotionsverfahren stattgefunden haben.

Ich erkenne die Promotionsordnung der Fakultät für Mathematik und Naturwissenschaften, Technische Universität Dresden an.

Samata Chaudhuri
Dresden, 19$^{\text{th}}$ October 2017